JOC The Journal of Organic Chemistry

pubs.acs.org/joc Article

Mechanistic Investigation of the Formation of Isoindole *N*-Oxides in the Electron Transfer-Mediated Oxidative Cyclization of 2′-Alkynylacetophenone Oximes

Wan Shin Kim, Victor M. Espinoza Castro, Amanda Abiad, Michael Ko, Ashley Council, Anh Nguyen, Laura Marsalla, Vicky Lee, Thao Tran, Andrew S. Petit,* and H. J. Peter de Lijser*

Cite This: *J. Org. Chem.* 2021, 86, 693−708 Read Online

ACCESS | Metrics & More | Article Recommendations | Supporting Information

ABSTRACT: This paper describes a joint experiment−theory investigation of the formation and cyclization of 2′-alkynylacetophenone oxime radical cations using photoinduced electron transfer (PET) with DCA as the photosensitizer. Using a combination of experimental ^{1}H and ^{13}C nuclear magnetic resonance (NMR) spectra, high-resolution mass spectrometry, and calculated NMR chemical shifts, we identified the products to be isoindole *N*-oxides. The reaction was found to be stereoselective; only one of the two possible stereoisomers is formed under these conditions. A detailed computational investigation of the cyclization reaction mechanism suggests facile C−N bond formation in the radical cation leading to a 5-exo intermediate. Back-electron transfer from the DCA radical anion followed by barrierless intramolecular proton transfer leads to the final product. We argue that the final proton transfer step in the mechanism is responsible for the stereoselectivity observed in experiment. As a whole, this work provides new insights into the formation of complex heterocycles through oxime and oxime ether radical cation intermediates produced via PET. Moreover, it represents the first reported formation of isoindole *N*-oxides.

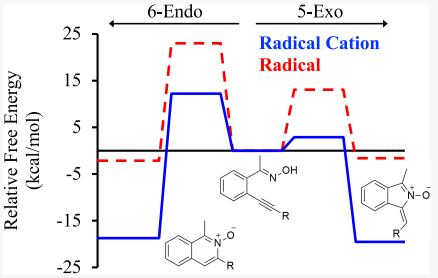

INTRODUCTION

Oxime-derived compounds have a broad range of applications such as industrial chemicals,[1−3] pharmaceuticals,[4−8] and antidotes for nerve gas poisoning.[9−12] Because oximes and oxime ethers contain two heteroatoms, they are popular reagents for the synthesis of heterocycles, including natural products and pharmaceuticals via intermolecular and intramolecular reactions.[13−21] We have previously reported on the use of 2′-arylbenzaldehyde oxime ethers as precursors for the synthesis of phenanthridine derivatives under photoinduced electron transfer (PET) conditions.[22] This work was based on the observation that oxime ether radical cations underwent intermolecular nucleophilic attack at the nitrogen,[23] whereas oximes did not show such reactivity but instead formed the corresponding carbonyl or nitrile via the proposed iminoxyl or iminoyl radicals.[24,25] The intermediate oxime radical cations are highly acidic and quickly lose a proton to form an iminoxyl radical, which might be more prone to react with a built-in radical trap.[22,26,27] Our initial study on the oxidative cyclization reactions of oximes and oxime ethers showed that built-in aromatic rings behaved as nucleophiles reacting with the nitrogen atom of the oxime ether moiety.[22] Because the oximes did not show such reactivity, it was proposed that aromatic rings do not act as radical traps. Unlike photochemical or metal-catalyzed reactions of similar substrates, the PET reaction was found to be selective (no nitrile byproduct was formed) as well as regiospecific when using 2′-aryl groups with meta-substituents.

To further explore the scope and limitations of oxidative cyclization reactions of oximes and oxime ethers under photoinduced electron transfer conditions, we have expanded our studies to investigate the behavior of the alkyne moiety as a nucleophile or a radical trap. Scheme 1 below summarizes the possible cyclization pathways under these specific assumptions. The alkyne moiety is expected to behave as a nucleophile in the case of radical cation intermediates, which would possibly lead to intermediate structures **I** or **II**. Alternatively, deprotonation of the oxime radical cation prior to nucleophilic attack by the alkyne will result in an iminoxyl radical, which may react with the alkyne moiety (as a radical trap) to yield cyclic structures such as **III** and **IV**.

Several groups have reported on the transformations of *ortho*-alkynylaryl oxime derivatives, including various metal-catalyzed processes.[28−35] In general and ignoring follow-up reactions, the main products observed in these types of

Received: September 29, 2020
Published: December 18, 2020

https://dx.doi.org/10.1021/acs.joc.0c02318
J. Org. Chem. 2021, 86, 693−708

Scheme 1. Possible Exo and Endo Cyclization Pathways of Oxime Radical Cations and Iminoxyl Radicals with the Built-In Alkyne Group Acting as a Nucleophile or Radical Trap

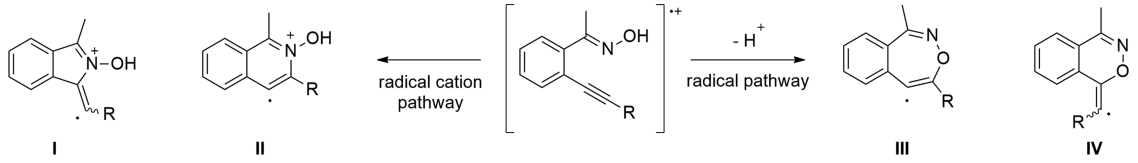

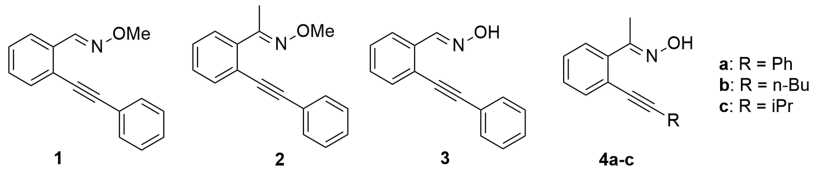

Figure 1. Structure of oxime and oxime ether substrates used in the photooxidative cyclization studies.

intramolecular cyclization reactions include isoquinoline *N*-oxides,[28−32] isoindoles,[33] isoquinolines,[34] isoquinolin-1(2H)-ones,[34] or indoles.[35]

Early reports showed the formation of isoquinoline *N*-oxides from *o*-alkynyl oximes using an acid catalyst and heat.[28,29] Under similar conditions, the methyl oxime ether was found to produce an isoquinoline product.

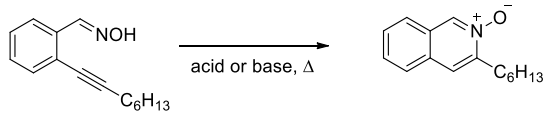

Wu and Ding demonstrated the formation of functionalized isoquinoline *N*-oxides via electrophilic cyclization of *o*-alkynylbenzaldehydes with various electrophiles.[30]

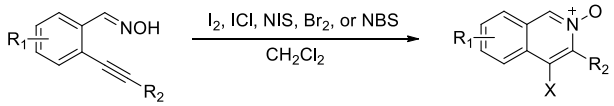

Similar reactions were reported by Yamamoto and co-workers.[31]

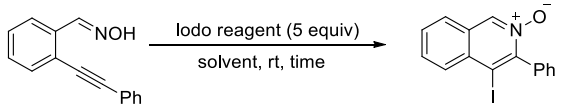

Shin and co-workers demonstrated the use of different transition metal catalysts for the formation of quinoline *N*-oxides from *o*-alkynyl oximes via 6-endo-dig N attack of the (*E*)-oxime.[32]

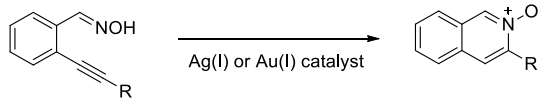

It was found that when using the *Z*-isomer of the oxime, the reaction produced predominantly or exclusively an isoindole product.[33]

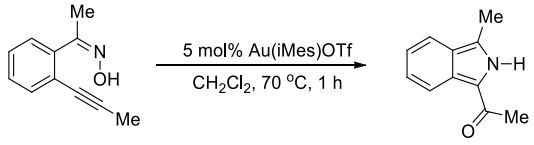

Zhang and Gao observed an interesting substituent effect in the silver(I)-catalyzed cyclization reaction of *o*-alkynyl benzaldehyde oxime derivatives, resulting in the formation of isoquinolines or isoquinolin-1(2H)-ones, depending on the oxime ether group.[34]

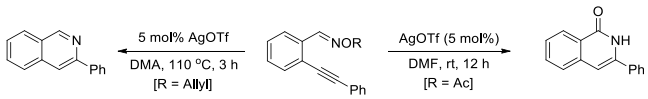

In the presence of cyanuric chloride, a Lewis acid ($InCl_3$), and a cocatalyst ($PdCl_2(MeCN)_2$), Wu and co-workers observed a Beckmann rearrangement/intramolecular cyclization reaction of ketoximes that resulted in the formation of substituted indoles.[35]

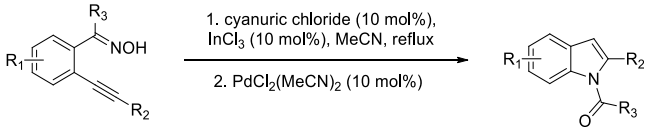

Given the differences that we observed between the metal-catalyzed cyclization reactions[36−38] and the oxidative cyclization reactions of the 2′-arylbenzaldehyde oxime ethers under PET conditions,[22] we set out to investigate the behavior of alkyne groups in a set of *ortho*-alkynyl benzaldehyde and acetophenone oximes and oxime ethers under PET conditions (see Figure 1). Our recent work has shown that radical cation intermediates are easily generated when using oxime ethers and 9,10-dicyanoanthracene (DCA) as the sensitizer[22] or with chloranil (CA) as the sensitizer.[24,26,27] However, previously, we have proposed that using CA as a sensitizer in the PET reactions of oximes results in the formation of iminoxyl radicals, presumably because the CA radical anion is a basic species and aids in the deprotonation of the oxime radical cation (as seen by formation of the semiquinone radical under those conditions).[27] Alternatively, because the DCA radical anion is not a strong base, using DCA as the photosensitizer could allow us to generate the oxime radical cations without facilitating the deprotonation step. This in turn would increase the lifetime of the radical cation intermediate, allowing for nucleophilic attack by the alkyne moiety. As such, we have carried out a series of preliminary studies to look at the effect of the sensitizer in these reactions. Furthermore, we have carried out blank experiments to eliminate any reactions that are due to direct light absorption by the oximes or oxime ethers. The results of these studies, combined with an in-depth theoretical analysis of the mechanistic aspects of these reactions, suggest the formation of a different product, an isoindole-*N*-oxide, which, to the best of our knowledge, is the first reported formation and isolation of this type of species.

https://dx.doi.org/10.1021/acs.joc.0c02318
J. Org. Chem. 2021, 86, 693−708

RESULTS AND DISCUSSION

Optimization of the Oxidative Cyclization Pathway. The desired alkynyl benzaldehydes and acetophenones as well as their oxime and oxime ether derivatives (Figure 1) were prepared according to standard literature methods with minor modifications.[37,38] Reactions were carried out on a small scale in NMR tubes using deuterated solvents in order to follow the reactions by NMR. Samples were also analyzed by GC−MS or LC−MS spectrometry to verify product formation.

To explore the use of the alkyne moiety as a nucleophile or a radical trap in the oxidative cyclization pathways of *o*-alkynyl benzaldehyde and acetophenone oximes and oxime ethers, conditions that were successful for similar reactions of 2′-biaryl oxime ethers were attempted first.[22] Irradiation of an acetonitrile solution containing oxime ether **1** and 9,10-dicyanoanthracene (DCA) as the sensitizer at 420 nm (Table 1, entry 1) resulted in degradation of the starting material with no indication of cyclization or other product formation. When the reaction was done with chloranil (CA) as the sensitizer at 350 nm (entry 2), the only reactivity observed was *E*/*Z* isomerization (as confirmed by the same reaction without CA present). Previously, we have observed that reactions of oximes and oxime ethers derived from aldehydes react slower than those derived from ketones.[23−27] Our next step, therefore, was to look at the reactivity of the corresponding acetophenone oxime ether (**2**). Reacting oxime ether **2** with DCA at 420 nm (entry 4) did not result in any significant product formation; again, degradation of the starting material was the main pathway. The same reaction with CA at 350 nm (entry 4) showed minor *E*/*Z* isomerization. Given the differences between the observed reactivities of the 2′-biaryl oxime ethers[22] and the *o*-alkynyl benzaldehyde and acetophenone oxime ethers, it seems evident that the alkyne moiety behaves differently compared to the aromatic ring.

Table 1. Summary of the Photooxidation Reactions Performed in This Study along with Their Outcomes

entry	oxime/oxime ether	sensitizer	λ (nm)[a]	outcome
1	**1**	DCA	420	degradation
2	**1**	CA	350	isomerization
3	**1**		350	isomerization
4	**2**	DCA	420	degradation
5	**2**	CA	350	isomerization
6	**2**		350	isomerization
7	**3**	CA	350	isomerization
8	**3**		350	isomerization
9	**3**	DCA	420	no reaction
10	**4a**	CA	350	isomerization
11	**4a**		350	isomerization
12	**4a**	DCA	420	cyclization
13	**4b**	DCA	420	cyclization
14	**4c**	DCA	420	cyclization

[a]The light output consists of a range of approximately 100 nm centered around the maximum output observed near either 350 nm (CA) or 420 nm (DCA).

In order for the oxidative cyclization to be successful, the radical cation intermediate must have a significant lifetime, which is why the use of oxime ethers was successful in the previous study.[22] Oxime radical cations are highly acidic and generally deprotonate quickly,[39,40] which typically prohibits attack by the built-in nucleophile. Deprotonation of the oxime radical cation yields an iminoxyl radical, which may react with a radical trap. To determine whether the alkyne moiety reacts as a radical trap rather than a nucleophile under these conditions, we prepared the *o*-alkynyl benzaldehyde and acetophenone oximes (**3** and **4a−c**) and subjected them to the PET conditions described above. To promote formation of the iminoxyl radicals, the reactions were carried out with chloranil (CA) as the sensitizer. The CA radical anion is known to be basic,[23−27] and spectroscopic studies have shown the formation of the semiquinone radical via proton transfer from an oxime radical cation to the CA radical anion.[27] Irradiation of oxime **3** at 350 nm in the presence of CA (Table 1, entry 7) resulted in the formation of new signals in the NMR spectrum. When the same reaction was done in the absence of CA, the same new signals were observed in the NMR spectrum, suggesting that these new signals were due to *E*/*Z* isomerization of the oxime. In the presence of DCA, oxime **3** did not show any reaction when irradiated at 420 nm.

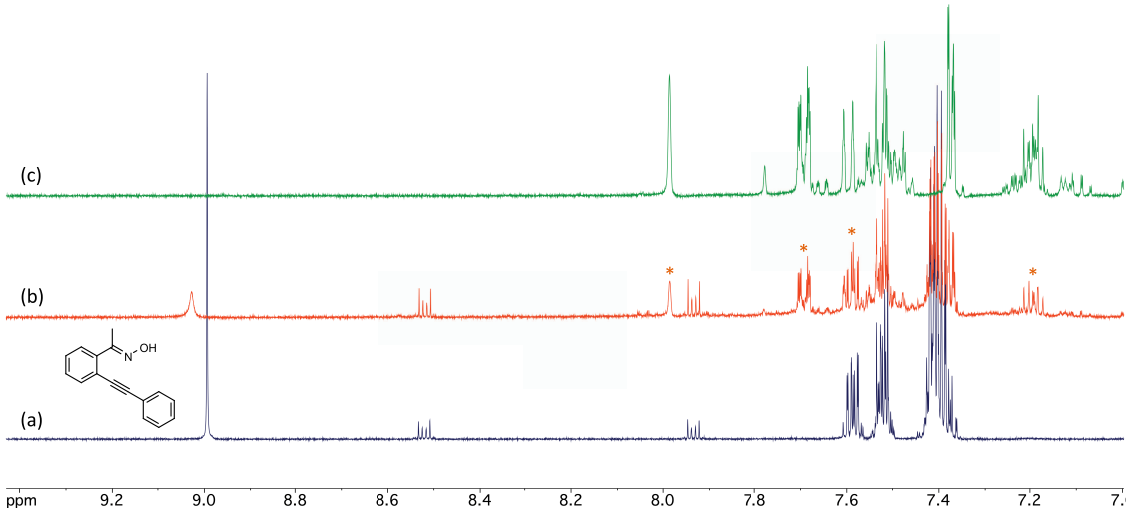

Figure 2. ^{1}H NMR spectra at 400 Hz of oxime **4a** with DCA in CD_3CN upon irradiation at 420 nm for (a) 0 and (b) 2 h. Signals growing in (at 7.98, 7.70, and 7.19 ppm) are marked with an asterisk. Isolated reaction product (c) showing signals that are consistent with the ingrowing signals.

https://dx.doi.org/10.1021/acs.joc.0c02318
J. Org. Chem. 2021, 86, 693−708

Scheme 2. Exo Cyclization (Right) and Endo Cyclization (Left) Pathways of *o*-Alkynylacetophenone Oxime Derivatives

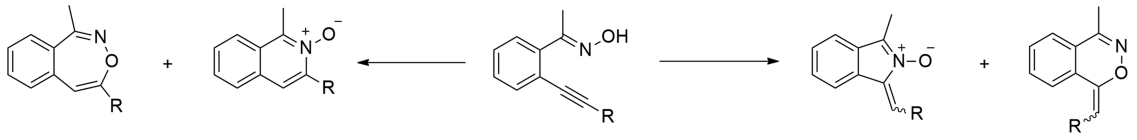

Scheme 3. Potential Products of the DCA-Catalyzed Photooxidative Cyclization of *o*-Alkynylacetophenone Oxime Derivatives for the Identification of Possible ^{1}H NMR Coupling Patterns

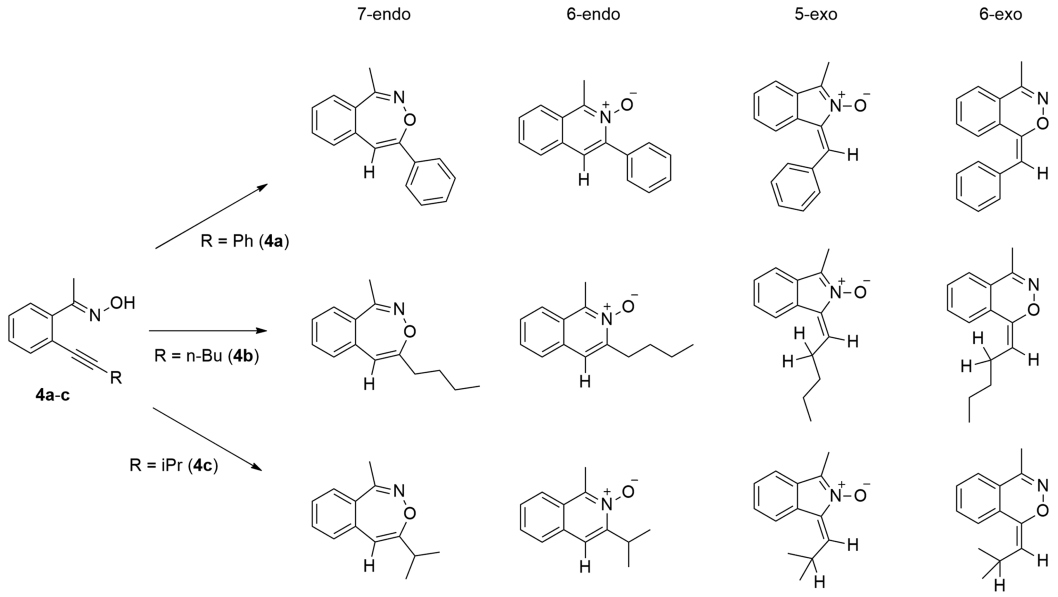

Table 2. Summary of Expected Splitting Patterns (s = Singlet; d = Doublet; t = Triplet; m = Multiplet) for the Potential Exo and Endo Products Derived from Photooxidative Cyclization Reactions of Oximes 4a−c

	7-endo	6-endo	5-exo	6-exo
	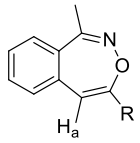	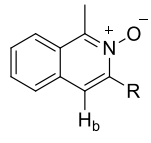	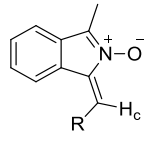	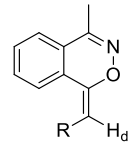
	H_a	H_b	H_c	H_d
4a (R = Ph)	s	s	s	s
4b (R = $CH(CH_3)_2$	s	s	t or m	t or m
4c (R = $(CH_2)_3CH_3$	s	s	d or m	d or m

Even after 4 h of irradiation, only a small amount of isomerization was observed. Irradiation of oxime **4a** at 350 nm (with or without CA) again resulted in isomerization of the starting material; however, when the oxime was irradiated at 420 nm in the presence of DCA (entry 12), several new signals (at 7.98, 7.70, and 7.19 ppm) were found to grow in over time, whereas the oxime signal (9.17 ppm) disappeared (Figure 2). After 2 h of irradiation, the conversion of the starting material into the new product was clear and fairly clean, but prolonged irradiation complicated a more detailed analysis of the reaction mixture.

Comparison of the signals seen in the reaction mixture (Figure 2b; t = 2 h) to those of the same reaction with CA at 350 nm shows that the new signals are not due to E/Z isomerization. Similarly, the new signals did not belong to the corresponding ketone compound, leaving cyclization as a potential pathway. A larger scale photolysis experiment allowed for isolation of the product (Figure 2c), which demonstrated that the peaks seen growing in belonged to the unknown product.[41] High-resolution mass spectrometry suggested no change in molecular formula for the product, consistent with the formation of a cyclic species via an intramolecular pathway, but complete characterization was not possible from the NMR and MS data.

Based on the existing literature of metal-catalyzed cyclization reactions of *o*-alkynyl benzaldehyde and acetophenone oximes,[13−21] as well as the previous work from our lab, which has suggested that the two main pathways involve

https://dx.doi.org/10.1021/acs.joc.0c02318
J. Org. Chem. 2021, 86, 693−708

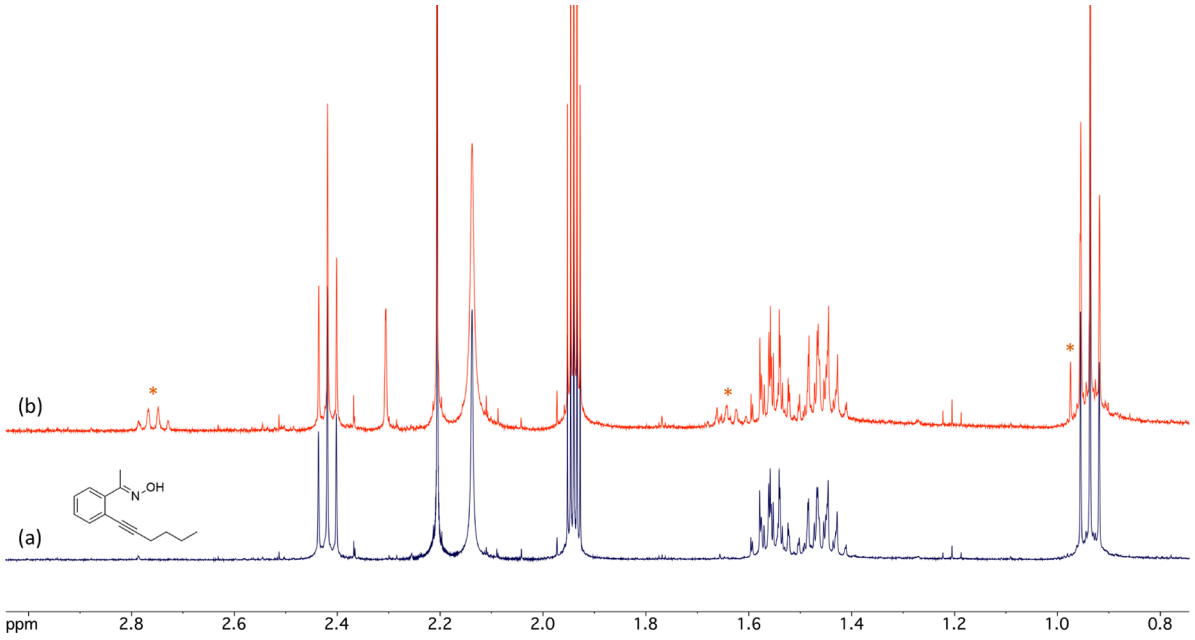

Figure 3. ^{1}H NMR spectra at 400 Hz of the aliphatic region of oxime **4b** with DCA in CD_3CN upon irradiation at 420 nm for (a) 0 and (b) 2 h. Signals growing in (at 0.95, 1.64, and 2.76 ppm) are marked with an asterisk. Attempts to isolate the reaction product were unsuccessful.

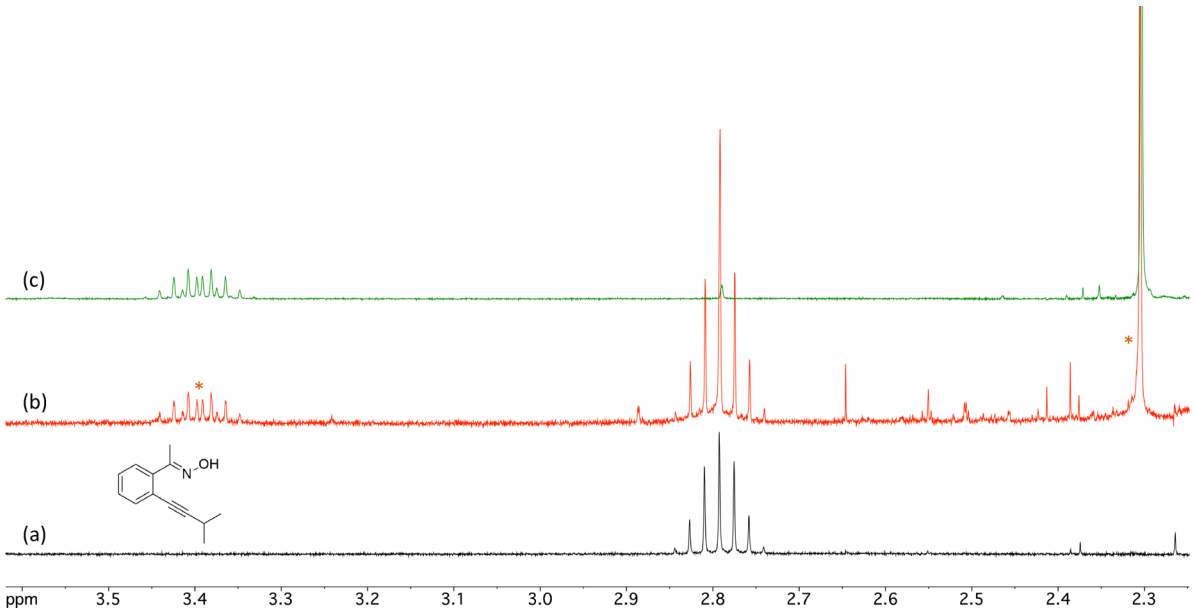

Figure 4. ^{1}H NMR spectra at 400 Hz of the aliphatic region of oxime **4c** with DCA in CD_3CN upon irradiation at 420 nm for (a) 0 and (b) 2 h. Signals growing in (at 3.39 and 2.29 ppm) are marked with an asterisk. Isolated reaction product (c) showing signals that are consistent with the ingrowing signals.

nucleophilic attack on the radical cation and radical trapping,[22] the main focus was on the 5-exo, 6-exo, 6-endo, and 7-endo pathways and products. Considering the different cyclization pathways and products that are possible (Scheme 2), it became evident that different substrates would need to be tested to rule out certain pathways and products.

Scheme 3 and Table 2 show that changing the phenyl group on the alkyne to an alkyl group, such as butyl or isopropyl, will allow us to distinguish between the endo and exo pathways. In the case of the butyl and isopropyl derivatives, the exo products would be expected to show coupling between the alkenyl proton and the allylic protons. In particular, Table 2 shows that the alkenyl proton would be expected to be split into a triplet or multiplet for the butyl derivative and into a doublet or multiplet for the isopropyl derivative if an exo product is formed. In contrast, in the endo products, this type of coupling would be absent, and the alkenyl proton would be a singlet (although long-range coupling cannot be ruled out beforehand). It should be noted that each of the exo products can exist as a cis or trans isomer (or a mixture); only the cis isomers are shown in Scheme 3 and Table 2.

Irradiation of oxime **4b** at 420 nm in the presence of DCA again resulted in the formation of new signals that are consistent with a cyclization pathway, similar to that of oxime **4a** (Figure 3). Analysis of the aromatic region of the NMR spectrum (Figure S1) shows the formation of a triplet signal

https://dx.doi.org/10.1021/acs.joc.0c02318
J. Org. Chem. 2021, 86, 693−708

Table 3. Comparison between the Experimental ^{1}H NMR Chemical Shifts of Compound 5a with the Calculated ^{1}H NMR Chemical Shifts of 5-Exo and 6-Exo Molecular Geometries

proton number[a]	region	experiment ^{1}H (ppm)	5-exo cis calculated ^{1}H (ppm)[b,c]	5-exo trans calculated ^{1}H (ppm)[b,c]	6-exo cis calculated ^{1}H (ppm)[b,c]	6-exo trans calculated ^{1}H (ppm)[b,c]
22	alkenyl	8.14 (1H)	8.14	7.22	6.46	6.11
15	aromatic	7.64−7.60 (3H)	7.86	7.59	7.49	7.64
19			7.76 (2H)	9.14 (2H)	7.33 (2H)	7.89 (2H)
20	aromatic	7.51−7.45 (3H)	7.51 (2H)	7.52 (2H)	7.25 (2H)	7.36 (2H)
21			7.48	7.58	7.41	7.53
17	aromatic	7.35−7.28 (2H)	7.28	7.32	7.37	7.39
18			7.15	7.21	7.30	7.35
16	aromatic	7.17 (1H)	7.09	7.27	7.21	7.18
23	methyl	2.48 (3H)	2.31 (3H)	2.39 (3H)	2.33 (3H)	2.32 (3H)

[a]The proton numbers are for the 5-exo cis geometry. The aromatic protons of the other geometries are ordered by chemical shift. [b]The number of equivalent hydrogens averaged together is given in parentheses. [c]NMR isotropic shielding tensors were calculated at the mPW1PW91/6-311+G(2d,p)//B3LYP/6-31+G(d,p) level of theory and converted into ^{1}H chemical shifts using the calibration curve developed by Pierens.[42]

(1H) at 7.04 ppm, which would be consistent with an aromatic or olefinic proton coupling to a methylene group. The aliphatic region (Figure 3) shows that the butyl group signals change over time with new signals growing in at 0.95, 1.64, and 2.76 ppm. The growth of a new quartet (2H) at 2.76 ppm is clear, and this splitting pattern would be most easily explained by a product formed via an exo pathway, with coupling between the allylic methylene protons and the olefinic exo proton. Attempts to isolate the product from the reaction mixture were not successful despite trying to do so under a variety of conditions.

Irradiation of oxime **4c** in acetonitrile in the presence of DCA at 420 nm shows the appearance of a doublet (1H) in the aromatic region (6.88 ppm, Figure S2) and a multiplet (1H) in the aliphatic region (3.39 ppm, Figure 4). HRMS analysis of the isolated product confirmed the mass of the alledged cyclic structure, but it is not possible to distinguish between endo or exo products. Further analysis of the ^{1}H NMR spectrum shows that it is consistent with that of a product formed via an exo cyclization pathway. The multiplet at 3.39 ppm contains two coupling constants: 6.67 and 10.56 Hz; the doublet at 6.88 ppm has a coupling constant of 10.56 Hz, which is consistent with a proton coupling to two equivalent methyl groups as well as a single olefinic (exo) proton.

These results confirm the above observation that the most likely explanation is an exo cyclization pathway to yield either an isoindole *N*-oxide or benzo[*d*][1,2]oxazine. To further rule out the endo pathways, we independently synthesized the isoquinoline *N*-oxides **6a−b** from oximes **4a−b**[32] and confirmed from their ^{1}H NMR spectra that they are not the products formed in the PET reactions (Figures S3 and S4 in the Supporting Information). We additionally subjected **4c** to the same conditions as were used to synthesize the isoquinoline *N*-oxides **6a−b** and confirmed that the resulting product has a distinctly different ^{1}H NMR spectrum (Figure S5) from the product formed through the PET reaction (Figure 4 and Figure S2).

Because the NMR and HRMS could not distinguish between the different exo products, we opted to further explore these two pathways by means of density functional theory in hopes of gaining a better understanding of the mechanistic aspects of these oxidative cyclization reactions.

Computational Analysis of the ^{1}H and ^{13}C NMR Chemical Shifts and Assignment of the 5a−5c Cyclized Products. The analysis shown in Table 2 and the NMR spectra shown in Figures 3 and 4 and Figures S1−S5 suggest that products **5a−5c** are the result of an exo cyclization pathway and distinct from the products of the Ag(I)-catalyzed oxidative cyclization of compounds **4a−4c**. However, they do not unambiguously identify whether **5a−5c** are the 5- or 6-exo cyclization products. In order to better understand the molecular structure of **5a−5c**, we turn to the computational prediction of the ^{1}H and ^{13}C NMR chemical shifts using the computational approach described in the Computational Methods. In order to first validate the chosen computational approach, we analyzed the ^{1}H and ^{13}C NMR chemical shifts of the isoquinoline *N*-oxide products **6a−6b** as well as an additional isoquinoline *N*-oxide from the literature,[33] the results of which are summarized in Tables S1−S6 in the Supporting Information. For these compounds, the calculated ^{1}H chemical shifts are all within 0.26 ppm of experiment, whereas the calculated ^{13}C chemical shifts are consistently within 3.44 ppm of experiment. This analysis provides a general sense of the accuracy that we can expect from the calculated NMR chemical shifts for conjugated *N*-oxides.

Table 3 compares the calculated ^{1}H NMR chemical shifts for potential 5-exo and 6-exo product molecular geometries with the experimental ^{1}H NMR chemical shifts of **5a**. The optimized 5-exo and 6-exo molecular geometries with the alkenyl hydrogen oriented cis with the N−O are shown in Figure 5; the 5-exo and 6-exo trans isomers, shown in Figure S9, have the phenyl group oriented cis with the N−O. The number of equivalent protons that were averaged together in the calculation of the chemical shifts is indicated in parentheses.

Table 3 shows that the calculated ^{1}H NMR chemical shifts for the 5-exo cis isomer are consistently in good agreement with experiment, with the largest discrepancy being 0.22 ppm. In particular, the calculated ^{1}H NMR chemical shift of the alkenyl proton for the 5-exo cis isomer is in excellent agreement with experiment. In contrast, the calculated alkenyl proton chemical shifts of the other three isomers exhibit large discrepancies with experiment, being too low by 0.92, 1.68, and 2.03 ppm for the 5-exo trans, 6-exo cis, and 6-exo trans isomers, respectively. It is important to note that the discrepancy between the experimental alkenyl proton NMR chemical shift and the calculated value for the 5-exo trans and 6-exo molecular geometries is significantly larger than the errors observed in the calculated ^{1}H NMR chemical shifts for the isoquinoline *N*-oxides (Tables S1−S6). As such, the data

https://dx.doi.org/10.1021/acs.joc.0c02318
J. Org. Chem. 2021, 86, 693−708

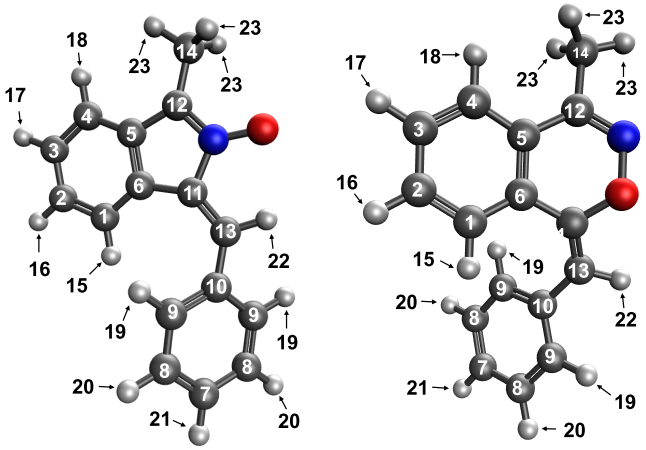

Figure 5. Optimized 5-exo (left) and 6-exo (right) molecular geometries with the alkenyl hydrogen oriented cis to the N−O group. The proton and carbon numbers referred to in Tables 3 and 4 are indicated. The geometries were optimized in the gas phase at the B3LYP/6-31+G(d,p) level of theory.

presented here is most consistent with **5a** being the 5-exo product with the alkenyl proton cis to the N−O.

Further support for our assignment of the molecular structure of **5a** comes from the ^{13}C NMR chemical shifts compared in Table 4. Focusing on the most downfield peaks, which are attributed to the two carbons that are adjacent to the N−O, the calculated chemical shifts for the 5-exo cis structure are in very good agreement with the experimental chemical shifts of **5a**, with differences of 0.28 and −0.06 ppm. In contrast, the calculated ^{13}C NMR chemical shifts for the 5-exo trans and both 6-exo molecular geometries are significantly further downfield than what is found in the experimental spectrum, with discrepancies of 5.25, 13.87, and 12.35 ppm for the 5-exo trans, 6-exo cis, and 6-exo trans molecular geometries. Turning to the rest of Table 4, the calculated chemical shifts of the 5-exo cis structure continue to be in good agreement with experiment, with the largest error being 1.69 ppm. Note, though, that assignment of the experimental alkenyl ^{13}C chemical shift is tentative because the calculated chemical shift of this carbon overlaps with the ^{13}C chemical shifts of other aromatic carbons.

Figures S10−S13 and Tables S7−S9 in the Supporting Information summarize our comparison between the calculated and experimental ^{1}H and ^{13}C NMR chemical shifts of products **5b** and **5c**. Throughout our analysis, we consistently find that the calculated chemical shifts of the 5-exo cis molecular geometry are in significantly better agreement with the experimental spectra than the other possible exo products. As above, this is especially true for the alkenyl proton and the carbons that are adjacent to the N−O. The largest discrepancies between the experimental chemical shifts of **5a−5c** and the calculated chemical shifts of the 5-exo cis geometry are 0.26 ppm for ^{1}H and 3.91 ppm for ^{13}C. Overall, our analysis based on the comparison of experimental and calculated ^{1}H and ^{13}C NMR data strongly suggests that products **5a−5c** have 5-exo molecular structures with the alkenyl hydrogen oriented cis to the N−O.

The Feasibility of Generating *o*-Alkynyl Oxime and Oxime Ether Radical Cations through PET. With solid support for the formation of products **5a−5c**, we now turn to understanding the mechanism through which they are formed, beginning with the photooxidative formation of the oxime radical cations through PET. Table 5 summarizes the experimental oxidation potentials of compounds **1−3** and **4a−4c**, along with the calculated change in free energy associated with PET, ΔG_{ET}, with either DCA or CA as the photosensitizer. For all compounds, ΔG_{ET} is less than 0, which indicates that formation of the radical cation through PET is spontaneous. When DCA is used as the photosensitizer, the range of ΔG_{ET} values is consistent with effective PET based on our previous study of the formation and intramolecular cyclization of 2′-arylbenzaldehyde oxime ether radical cations.[22,43] When CA is used as the photosensitizer, the ΔG_{ET} becomes even more negative. Based on our previous work, the use of CA with compounds **1−4a** results in ΔG_{ET}

Table 4. Comparison between the Experimental ^{13}C NMR Chemical Shifts of Compound 5a with the Calculated ^{13}C NMR Chemical Shifts of 5-Exo and 6-Exo Molecular Geometries

carbon number[a]	region	experiment ^{13}C (ppm)	5-exo cis calculated ^{13}C (ppm)[b,c]	5-exo trans calculated ^{13}C (ppm)[b,c]	6-exo cis calculated ^{13}C (ppm)[b,c]	6-exo trans calculated ^{13}C (ppm)[b,c]
12	N−O adjacent	142.79	143.07	148.04	156.66	155.14
11	N−O adjacent	141.38	141.32	139.33	149.32	150.01
13	alkenyl	129.70	131.13	128.75	110.63	102.45
5	aromatic	134.87	135.59	136.65	136.43	135.82
10	aromatic	133.02	133.70	132.65 (2C)	131.88	133.37
9	aromatic	129.84	130.83 (2C)	132.48	129.71	129.43
7	aromatic	129.83	130.38	132.02	128.57 (2C)	128.87
3	aromatic	128.92	129.32	130.02	128.50	128.69 (2C)
8	aromatic	128.85	128.48 (2C)	128.09 (2C)	128.41 (2C)	128.04 (2C)
6	aromatic	128.16	126.52	127.99	126.63	125.37
2	aromatic	126.71	126.22	126.20	125.82	124.82
1	aromatic	121.83	120.73	118.03	124.15	122.09
4	aromatic	119.22	117.53	117.17	123.78	120.26
14	methyl	9.76	9.84	10.68	17.14	17.36

[a]The carbon numbers are for the 5-exo cis geometry. The aromatic carbons of the other geometries are ordered by chemical shift. [b]The number of equivalent carbons averaged together is given in parentheses. [c]NMR isotropic shielding tensors were calculated at the B3LYP/6-311+G(2d,p)//B3LYP/6-31+G(d,p) level of theory and converted into ^{13}C chemical shifts using the calibration curve developed by Pierens.[42]

https://dx.doi.org/10.1021/acs.joc.0c02318
J. Org. Chem. 2021, 86, 693−708

Table 5. Experimentally Determined Oxidation Potentials (E^{OX}), Free Energies of Photoinduced Electron Transfer with DCA or CA as the Photosensitizer (ΔG_{ET}), and Calculated Ionization Potentials (IP) of Compounds 1−3 and 4a−4c

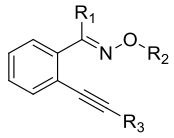

	R_1	R_2	R_3	E^{ox} (V)[a]	ΔG_{ET}[b] (kcal mol^{-1})	ΔG_{ET}[c] (kcal mol^{-1})	IP[d] (kcal mol^{-1})
1	H	CH_3	Ph	1.66	−6.9	−10.6	147.22
2	CH_3	CH_3	Ph	1.61	−8.0	−11.7	147.59
3	H	H	Ph	1.70	−5.9	−9.6	147.02
4a	CH_3	H	Ph	1.64	−7.4	−11.1	147.76
4b	CH_3	H	$CH_2CH_2CH_2CH_3$	1.78	−4.1	−7.7	151.75
4c	CH_3	H	$CH(CH_3)_2$	1.73	−5.2	−8.9	152.65

[a]Oxidation potentials (half-wave potentials) obtained by cyclic voltammetry. [b]Calculated free-energy changes for the one-electron transfer process from the compounds to ^{1}DCA* in acetonitrile by the application of the Rehm−Weller equation: the excited singlet energy of DCA, 2.90 eV, and reduction potential of DCA, −0.91 V vs SCE.[44,45] [c]Calculated free-energy changes for the one-electron transfer process from the compounds to ^{3}CA* in acetonitrile by the application of the Rehm−Weller equation: the excited triplet energy of CA, 2.13 eV, and reduction potential of CA, 0.02 V vs SCE.[44,45] [d]Calculated ionization potentials at the ωB97M-V/def2-QZVPP//ωB97X-D/cc-pvdz level of theory.[43]

values that lie deep in the Marcus inverted region where PET will occur very slowly, if at all. This potentially explains why only isomerization was observed when CA was used as the photosensitizer with these compounds.

Focusing on compounds **4a−4c** with DCA, the ΔG_{ET} of **4a**, −7.4 kcal/mol, is considerably more negative than the ΔG_{ET} of **4b** and **4c**, −4.1 and −5.2 kcal/mol, respectively. In order to understand the cause of this, we analyzed the spin densities, which indicate where the unpaired electron is localized in the radical cation and hence where the oxidation primarily occurred. The spin densities of the radical cations at the neutral optimized geometries of **4a−4c** are reported in Figure S14 in the Supporting Information. For compounds **4b** and **4c**, the spin density is found to be primarily localized on the central benzene ring and alkynyl group, with little spin density present on the oxime group. In contrast, for compound **4a**, the spin density is further delocalized into the phenyl group, stabilizing the radical cation and hence lowering the oxidation potential.

Table 5 provides additional insights into the pattern of reactivity summarized in Table 1. In particular, the fact that compounds **1−3** all have ΔG_{ET} that are more negative than those of **4b−4c** suggests that compounds **1−3** can undergo PET with DCA. As a result, the inability of compounds **1−3** to undergo cyclization cannot be attributed to radical cation formation but rather to subsequent steps in the mechanism.

Computational Analysis of the Radical Cation Cyclization Mechanism. With the formation of the radical cations discussed, we now consider their reactivity, focusing first on the ketone oximes. Oxime radical cations are well-known to be strongly acidic, and the compounds considered in this study are no exception.[39,40] Indeed, the calculated pK_a values for the **4a−4c** radical cations range from −6.41 to −9.81, suggesting that a large fraction of the radical cations generated through PET will undergo deprotonation to form iminoxyl radicals; further details may be found in Table S10 in the Supporting Information. As such, we will consider the possibility of both radical cation and iminoxyl radical cyclization in our analysis.

According to our analysis of the NMR spectra, the most likely cyclization pathway of compounds **4a−4c** leads to the 5-exo product (**5a−5c**) in each case. Figure 6 shows the reaction

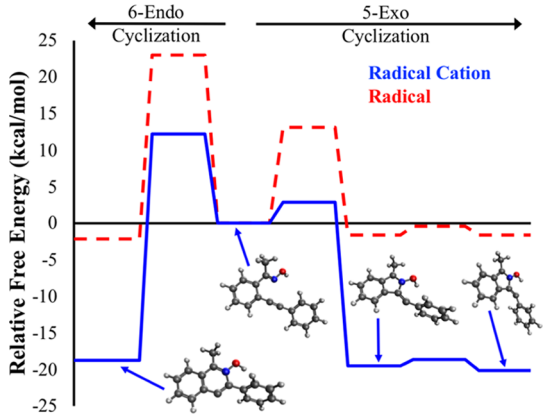

Figure 6. 5-Exo and 6-endo cyclization reaction coordinate diagrams for the radical cation (solid blue line) and the iminoxyl radical (dashed red line) of **4a**. All free energies were evaluated at the RO-ωB97M-V/def2-QZVPP//U-ωB97X-D/cc-pVDZ level of theory and are reported relative to the lowest energy acyclic radical cation or radical conformation.

coordinate diagram for the formation of the 5-exo intermediates as both an iminoxyl radical (dashed red line) and as a radical cation (solid blue line) for compound **4a**. The free energies are reported relative to the lowest acyclic minimum energy geometry of the radical or radical cation, both of which have the nitrogen of the oxime group oriented toward the alkynyl group. The radical pathway for 5-exo cyclization has a free-energy barrier of 13.1 kcal/mol and results in an intermediate that is downhill in free energy by −1.6 kcal/mol. In contrast, the radical cation has a very low barrier for 5-exo cyclization of only 2.9 kcal/mol. Moreover, the radical cation 5-exo intermediate is much lower in free energy than the corresponding radical intermediate at −20.1 kcal/mol. For both the iminoxyl radical and the radical cation, the 5-exo intermediate can exist in two isomers, which are nearly isoenergetic and separated by a small, less than 1.5 kcal/mol, barrier. Figures S15 and S16 in the Supporting Information show very similar reaction coordinate diagrams for the 5-exo cyclization of **4b** and **4c**, with 5-exo cyclization more kinetically and thermodynamically favorable for the oxime radical cation than for the iminoxyl radical. Indeed, 5-

https://dx.doi.org/10.1021/acs.joc.0c02318
J. Org. Chem. 2021, 86, 693−708

exo cyclization is uphill in free energy by 2−4 kcal/mol for the iminoxyl radicals of compounds **4b** and **4c**.

Figure 6 also displays the reaction coordinate diagram for 6-endo cyclization, leading to **6a**. This pathway has a higher barrier than that leading to the 5-exo intermediate for both the iminoxyl radical and the radical cation, 23.0 and 12.2 kcal/mol, respectively. The 6-endo intermediate is similarly downhill in energy compared to the 5-exo intermediate for both the radical, −2.1 kcal/mol, and the radical cation, −18.7 kcal/mol. Figures S15 and S16 show that for **4b** and **4c**, formation of the 6-endo radical cation intermediate is more thermodynamically favorable than formation of the 5-exo radical cation intermediate. However, the barrier for 6-endo cyclization remains significantly larger than the barrier for 5-exo cyclization. As such, Figure 6 and Figures S15 and S16 suggest that 6-endo cyclization results in the thermodynamic product, whereas 5-exo cyclization leads to the kinetic product.

Figure 7 shows the reaction coordinate diagram for forming the 6-exo and the 7-endo intermediates as either a radical cation or an iminoxyl radical for compound **4a**. Both the 6-exo and 7-endo cyclization pathways begin from the acyclic *Z*-isomer conformation with the oxime group oriented toward the alkynyl group. For both the iminoxyl radical and the radical cation, there is an energetic cost to reaching the *Z*-isomer of the oxime group, which is necessary for C−O bond formation to occur. Moreover, the calculated barriers for the *E*/*Z* isomerization of the oxime group are 20.7 and 13.2 kcal/mol for the radical cation and the iminoxyl radical of compound **4a**, respectively. 7-Endo cyclization is uphill in free energy for both the radical and the radical cation and has a larger barrier than 6-exo cyclization. As a radical cation, 6-exo cyclization has a free-energy barrier of 11.3 kcal/mol and results in a 6-exo radical cation intermediate that is uphill in free energy by 9.2 kcal/mol. In contrast, as an iminoxyl radical, the 6-exo intermediate is downhill in free energy by −3.0 kcal/mol but separated from the acyclic conformation by a 17.8 kcal/mol barrier. Figures S17 and S18 show that the reaction coordinate diagrams associated with C−O bond formation as a radical cation or an iminoxyl radical for **4b** and **4c** are similar to that shown in Figure 6; the only major difference is that the 6-exo intermediates of **4b** and **4c** are uphill in free energy for both the radical cation, 9.0−10.6 kcal/mol, and the radical, 3.2−5.2 kcal/mol. Collectively, Figures 6 and 7 and Figures S15−S18 show that C−O bond formation is less kinetically and thermodynamically favorable than C−N bond formation for compounds **4a**−**4c**.

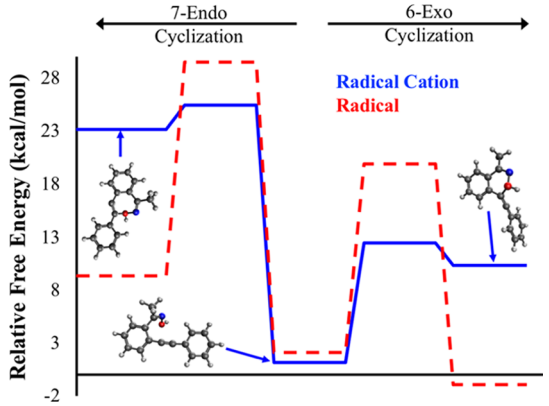

Figure 7. 6-Exo and 7-endo cyclization reaction coordinate diagrams for the radical cation (solid blue line) and the iminoxyl radical (dashed red line) of **4a**. All free energies were evaluated at the RO-ωB97M-V/def2-QZVPP//U-ωB97X-D/cc-pVDZ level of theory and are reported relative to the lowest energy acyclic radical cation or radical conformation.

In order to understand the difference in reactivity between the radical cation and the radical, we analyzed the natural bond orbital (NBO) spin densities and partial charges at the radical and radical cation acyclic conformers with the oxime nitrogen oriented toward the alkynyl group;[46] this information is summarized in Tables S11 and S12 in the Supporting Information. For the radical compounds, the NBO spin density is strongly localized on the N and O, with the N becoming electrophilic due to its positive NBO partial charge. In contrast, the NBO spin density of the radical cations is most strongly localized on the alkynyl group, with little NBO spin density localized on O. This is consistent with the spin density distributions at the neutral optimized conformations shown in Figure S14. For the **4b** and **4c** radical cations, the spin density on the N is comparable in magnitude to that localized on the alkynyl carbon closest to the oxime group, whereas for the **4a** radical cation, little spin density is localized on the N. For all of the radical cations, the alkynyl carbons bear either positive or slightly negative partial charges, whereas the NBO partial charge on N is significantly more negative. Overall, the data summarized in Tables S11 and S12 suggests that the reaction coordinate diagrams are different for the radical and the radical cation because of differences in how the unpaired electron is distributed in the molecule. Moreover, both the radical cation spin densities and charge distributions are inconsistent with the alkynyl group acting as a nucleophile. Finally, note that for the radical cations, the proton on the oxime group is calculated to have a large NBO partial charge, 0.51 to 0.52, which is consistent with the strong acidity of these oxime radical cations shown in Table S10.

Overall, the cyclization pathway is most consistent with the involvement of a radical cation intermediate and the formation of the 5-exo products **5a**−**5c**. Figure 6 demonstrates that the kinetic as well as thermodynamic driving forces are both significantly larger for radical cation cyclization than for radical cyclization. Moreover, for the radical cations, cyclization must compete with deprotonation, and because deprotonation is thermodynamically very favorable, radical cation cyclization must occur extremely rapidly to occur prior to deprotonation. This provides an explanation for why **5a**−**5c** are the kinetic 5-exo cyclic products rather than the thermodynamic 6-endo cyclic products.

In Figure 8, we propose an overall mechanism for the PET-induced cyclization of compounds **4a**−**4c**. The initial steps in this mechanism, radical cation formation through PET with DCA and the subsequent intramolecular cyclization of the radical cation to generate the radical cation 5-exo cyclic intermediate, have been discussed above. The next step in the proposed mechanism involves back-electron transfer from the DCA radical anion to generate a neutral cyclic intermediate and DCA. As the PET required an input of 2.90 eV of energy to occur, this back-electron transfer will be thermodynamically favorable. Moreover, as DCA was previously shown to act as a catalyst in the photooxidative cyclization of 2′-arylbenzaldehyde oxime ethers,[22] it is reasonable to suggest that it acts as a catalyst in the photooxidative cyclization reaction studied here. Finally, because the minimum-energy acyclic conformer of the radical cation is already properly oriented for C−N bond

https://dx.doi.org/10.1021/acs.joc.0c02318
J. Org. Chem. 2021, 86, 693−708

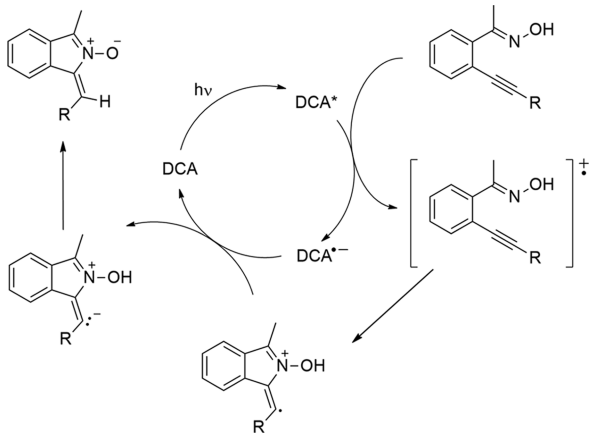

Figure 8. Proposed mechanism for the formation of isoindole *N*-oxides from the photooxidative cyclization of 2′-alkynylacetophenone oximes.

formation and the 5-exo cyclization barrier is very small, the radical cation cyclization will occur extremely rapidly. As such, it is possible that the 5-exo cyclic radical cation intermediate can form before the DCA radical anion has had enough time to diffuse away, further facilitating back-electron transfer.

A key aspect to the mechanism presented in Figure 8 is its account of how proton transfer from the oxime group to the divalent alkenyl carbon results in regioselectivity. While the acyclic radical cation is highly acidic, the 5-exo cyclic radical cation intermediate is a very weak acid; for the phenyl substituted oxime, the calculated pK_a is −6.41 for the acyclic radical cation and +8.23 for the 5-exo radical cation intermediate (see Table S10). However, the 5-exo neutral intermediate with the divalent alkenyl carbon oriented toward the oxime group was not a stable minimum energy geometry; upon optimization, the oxime proton always transferred to the divalent alkenyl carbon regardless of the initial orientation of the N−OH moiety. The final step in the mechanism presented in Figure 8 is therefore intramolecular proton transfer, which based on our computational results, is barrierless. Note that this intramolecular proton transfer necessarily results in only forming the 5-exo product with the alkenyl proton oriented cis to the N−O. In contrast, a radical cyclization mechanism provides no means for a stereoselective protonation; the two radical 5-exo intermediates are nearly isoenergetic, and hence, if they were formed, then **5a**−**5c** would be a mixture of cis and trans isomers, which is inconsistent with the experimental NMR spectra.

With the mechanistic pathway responsible for the generation of products **5a**−**5c** described, we now consider alternative pathways that will compete with the mechanism shown in Figure 8. As mentioned above, the acyclic radical cation conformations are highly acidic. As a result, radical cation cyclization must compete with deprotonation; despite the very low cyclization barrier and favorable cyclization thermodynamics, the strong acidity of the radical cations suggests that deprotonation of the radical cations generated through PET prior to cyclization is a competitive pathway. Previous research has shown that iminoxyl radicals can react via several pathways sometimes leading to complicated reaction mixtures, which is consistent with our observations in these experiments. For those radical cations that cyclize into a 5-exo intermediate, Figure 6 demonstrates that there are two nearly isoenergetic isomers that will be populated, only one of which can ultimately lead to product formation. Figure S20 in the Supporting Information shows that after back-electron transfer with the DCA radical anion, the 5-exo trans neutral intermediate will undergo C−N bond cleavage to regenerate the starting material. This process is kinetically and thermodynamically favorable; the barrier is 8.8 kcal/mol, and regeneration of the starting material is downhill in free energy by −18.5 kcal/mol for compound **4a**; the process is even more favorable for **4b** and **4c**. Likewise, Figure S21 shows that if the 6-endo radical cation intermediate is formed, then it will also undergo spontaneous C−N bond cleavage to regenerate the starting material after back-electron transfer makes it neutral; the barrier is less than 15 kcal/mol for all three compounds, and the C−N bond cleavage is downhill in free energy by −14.2 to −15.9 kcal/mol.

The proposed mechanism of the radical cation cyclization of compounds **4a**−**4c** also explains why no product formation was observed for the oxime ethers **1** and **2**. As discussed above, Table 5 shows that the ΔG_{ET} of compounds **1** and **2** is consistent with radical cation generation when DCA is the sensitizer. Likewise, our calculations suggest that radical cation 5-exo cyclization will occur; further details are shown in Figures S22 and S23 in the Supporting Information. However, formation of the final product now requires an intramolecular methyl group transfer as opposed to an intramolecular proton transfer. This methyl group migration is expected to have a very high barrier, making it kinetically unfeasible. Instead, the neutral 5-exo intermediate, formed after back-electron transfer with the DCA radical anion, undergoes C−N bond dissociation to regenerate the starting material; see Figure S24 in the Supporting Information.

We finally consider why no product is observed with compound **3**. Table 5 shows that the ΔG_{ET} of compound **3** is more negative than those of **4b** and **4c**, suggesting that compound **3** will undergo PET with DCA. Figures S25 and S26 in the Supporting Information suggest less favorable radical cation cyclization kinetics for compound **3** than for compound **4a**. Specifically, Figure S26 shows that the two acyclic radical cation conformers of **3** are essentially isoenergetic with no significant thermodynamic driving force to align the oxime and alkynyl groups for cyclization. In contrast, the acyclic radical cation conformer of **4a** with the N oriented toward the alkynyl group is 1.98 kcal/mol lower in energy than the other conformer. Moreover, the radical cation 5-exo cyclization barrier for **3** is higher than for **4a**, 5.14 kcal/mol versus 2.91 kcal/mol. Collectively, this suggests that the radical cation form of compound **3** will require more time for the oxime and alkynyl groups to align themselves and subsequently cyclize than the radical cation form of compound **4a**. This will make radical cation deprotonation more competitive with cyclization for compound **3**, potentially to a large enough extent to explain the absence of the product with this compound.

CONCLUSION

In this paper, we discussed our study of the generation of isoindole *N*-oxides from the PET-induced cyclization of *ortho*-alkynylaryl oximes. This represents the first reported formation of such compounds as well as demonstrates that the photooxidative cyclization of 2′-alkynylacetophenone oximes results in a different product from that in previously reported metal-catalyzed cyclization reactions. Moreover, the cyclization

https://dx.doi.org/10.1021/acs.joc.0c02318
J. Org. Chem. 2021, 86, 693−708

reaction reported in this study is fully stereoselective, with only a single isomer of the isoindole *N*-oxides formed.

A detailed computational investigation of the reaction mechanism revealed that the barrier for 5-exo radical cation cyclization is very low, less than 3 kcal/mol, allowing radical cation cyclization to compete with deprotonation. Moreover, the formation of the 5-exo radical cation intermediate is thermodynamically favorable by at least −19 kcal/mol. Back-electron transfer from the DCA radical anion results in a neutral intermediate, which subsequently undergoes intramolecular proton transfer to generate the final product. We demonstrated that the stereoselectivity of the overall cyclization reaction originates from the need for the oxime group and the divalent alkenyl carbon to be oriented toward each other in the neutral intermediate in order for the intramolecular proton transfer to occur; all other intermediates were shown to regenerate the starting material after back-electron transfer.

EXPERIMENTAL SECTION

General Information. All chemicals were obtained from commercial sources and used as supplied without further purification unless otherwise noted. 9,10-Dicyanoanthracene (DCA) was recrystallized from pyridine at 80 °C. All aqueous bases were prepared by dissolving the appropriate amount of solid by mass into a volumetric flask before being diluted with distilled water and degassed with heat and agitation under vacuum. All new compounds were characterized by ^{1}H NMR,^{13}C NMR, and high-resolution mass spectrometry. Known compounds were characterized by ^{1}H NMR and ^{13}C NMR and compared to their literature values. NMR spectra were recorded on a 400 MHz (^{1}H at 400 MHz, ^{13}C at 100 MHz) instrument and obtained with ^{1}H decoupling. The data are reported as follows: chemical shift (multiplicity, coupling constant in Hz, integration). Multiplicities are abbreviated as follows: s = singlet, d = doublet, t = triplet, q = quartet, quint = quintet, sept = septet, m = multiplet, and br = broad. All ^{1}H NMR spectra are reported in δ (ppm) units and are relative to residual solvent signals of $CDCl_3$ (7.26 ppm) or CD_3CN (1.94 ppm). All ^{13}C NMR spectra are reported in δ (ppm) units and are relative to residual $CDCl_3$ (77.0 ppm) solvent signals. High-resolution mass spectra were obtained using a Thermo Scientific Q Exactive Focus benchtop quadrupole Orbitrap high-resolution mass spectrometer.

Oxidation Potentials. Cyclic voltammetry was used to determine oxidation potentials of the oxime ethers dissolved in acetonitrile with tetraethylammonium perchlorate (0.1 M) as the electrolyte. Solutions were degassed under an argon atmosphere and scanned at a rate of 100 mV/s against a Ag/AgCl reference electrode. The experimental oxidation potentials were converted into free energies of electron transfer, ΔG_{ET}, using the Rehm−Weller equation, $\Delta G_{ET} = E^{ox} - E^{red} - h\nu$.[44,45] The E^{red} of DCA and CA were adjusted by −0.014 V to correct for the fact that literature reduction potentials were measured against SCE whereas a Ag/AgCl reference electrode was used in this study. A +0.044 V correction factor was applied to the measured E^{ox} to account for the fact that they are peak potentials for an irreversible system as opposed to the actual oxidation potentials.[47,48]

General Procedure for the Synthesis of *o*-Alkynylbenzaldehyde and Acetophenones. A 30 mL pressure tube with a screw-top was evacuated and backfilled with argon prior to the addition of 2-bromobenzaldehyde or 2-iodoacetophenone (5.0 mmol, 1 equiv), appropriate alkyne (7.5 mmol, 1.5 equiv), triphenylphosphine (0.12 mmol, 2.5 mol %), and triethylamine (7.5 mmol, 1.5 equiv) in anhydrous tetrahydrofuran (10 mL). The mixture was allowed to stir for 10 min, after which bis(triphenylphosphine)palladium(II) chloride (0.25 mmol, 5.0 mol %) and copper(I) iodide (0.5 mmol, 10 mol %) were added. The mixture was heated in an oil bath and stirred for 24 h. Afterward, the mixture was diluted with ethyl acetate and vacuum-filtered using celite. The solution was extracted with water and brine and dried over sodium sulfate. After concentration *in vacuo*, the resulting crude mixture was purified using combiflash with ethyl acetate/hexane as the eluting solvent.

2-(Phenylethynyl)benzaldehyde.[49] 2-Bromobenzaldehyde (0.995 g, 5.4 mmol), ethynyl benzene (0.765 g, 7.5 mmol), anhydrous tetrahydrofuran (10 mL), triphenylphosphine (2.5 mol %), and triethylamine (1.5 mol equiv) were added to an argon-purged pressure tube. The mixture was stirred for 10 min, after which bis(triphenylphosphine)palladium(II) chloride (0.175 g, 5 mol %) and copper(I) iodide (0.095 g, 9 mol %) were added. The mixture was heated to 85 ° C and stirred for 24 h. Afterward, the mixture was diluted with ethyl acetate (15 mL), extracted with water (3 × 30 mL) and brine (2 × 30 mL), and dried over sodium sulfate. The concentrated mixture was purified by column chromatography with ethyl acetate (5%)/hexane (95%) as the eluting solvent to yield the product as an oil (0.4517 g, 41%). ^{1}H NMR (400 MHz, $CDCl_3$): δ 10.66 (d, J = 0.8 Hz, 1H), 7.96 (dd, J = 7.8, 0.9 Hz, 1H), 7.65 (ddd, J = 7.7, 1.3, 0.5 Hz, 1H), 7.61−7.56 (m, 3H), 7.48−7.44 (m, 1H), 7.41−7.38 (m, 3H). ^{13}C NMR (101 MHz, $CDCl_3$): δ 191.89, 136.00, 133.94, 133.38, 131.83, 129.23, 128.77, 128.68, 127.43, 127.04, 122.49, 96.48, 85.03.

1-(2-(2-Phenylethynyl)phenyl)ethenone.[49] 2-Iodoacetophenone (0.995 g, 4.0 mmol), ethynyl benzene (0.765 g, 7.5 mmol), and triethylamine (1.5 mol equiv) were added to an argon-purged pressure tube. The mixture was stirred for 10 min, after which bis(triphenylphosphine)palladium(II) chloride (0.175 g, 6 mol %) and copper(I) iodide (0.095 g, 12 mol %) were added. The mixture was heated to 50 °C and stirred for 24 h. Afterward, the mixture was vacuum-filtered with celite, diluted with ethyl acetate (15 mL), extracted with water (3 × 30 mL) and brine (2 × 30 mL), and dried over sodium sulfate. The concentrated mixture was purified using a combiflash with ethyl acetate (10%)/hexane (90%) as the eluting solvent to yield the product as a yellow oil (0.4517 g, 41%). ^{1}H NMR (400 MHz, $CDCl_3$): δ 7.76 (dd, J = 7.8, 1.2 Hz, 1H), 7.64 (dd, J = 7.7, 1.0 Hz, 1H), 7.56 (ddt, J = 5.5, 2.7, 1.4 Hz, 2H), 7.48 (td, J = 7.6, 1.5 Hz, 1H), 7.43−7.35 (m, 4H), 2.80 (s, 3H). ^{13}C NMR (101 MHz, $CDCl_3$): δ 200.56, 140.93, 134.03, 131.67, 131.45, 128.92, 128.84, 128.62, 128.43, 123.04, 121.85, 95.18, 88.62, 30.17.

1-(2-(Hex-1-yn-1-yl)phenyl)ethenone.[49] 2-Iodoacetophenone (0.902 g, 3.6 mmol), 1-hexyne (0.745 g, 9.0 mmol), and triethylamine (10 mL, 3.0 mol equiv) were added to an argon-purged pressure tube. The mixture was stirred for 10 min, after which bis(triphenylphosphine)palladium(II) chloride (0.175 g, 7 mol %) and copper(I) iodide (0.095 g, 14 mol %) were added. The mixture was heated to 50 °C and stirred for 24 h. Afterward, the mixture was vacuum-filtered with celite, diluted with ethyl acetate (15 mL), extracted with water (3 × 30 mL) and brine (2 × 30 mL), and dried over sodium sulfate. The concentrated mixture was purified by combiflash with ethyl acetate (10%)/hexane (90%) as the eluting solvent to yield the desired product as an oil (0.3332 g, 33%). ^{1}H NMR (400 MHz, $CDCl_3$): δ 7.65 (ddd, J = 7.8, 1.5, 0.5 Hz, 1H), 7.48 (ddd, J = 7.7, 1.4, 0.3 Hz, 1H), 7.39 (td, J = 7.5, 1.5 Hz, 1H), 7.32 (td, J = 7.6, 1.4 Hz, 1H), 2.72 (s, 3H), 2.46 (t, J = 7.1 Hz, 2H), 1.65−1.58 (m, 2H), 1.53−1.44 (m, 2H), 0.95 (d, J = 14.6 Hz, 3H). ^{13}C NMR (101 MHz, $CDCl_3$): δ 201.2, 141.2, 134.1, 131.2, 128.4, 127.6, 122.6, 97.0, 79.8, 30.7, 30.2, 22.2, 19.5, 13.7.

1-(2-(3-Methylbut-1-ynyl)phenyl)ethanone. 2-Iodoacetophenone (0.109 g, 0.44 mmol), 3-methylbutyne (0.052 g, 0.8 mmol), and triethylamine (5 mL) were added to an argon-purged pressure tube. The mixture was stirred for 10 min, after which bis(triphenylphosphine)palladium(II) chloride (0.017 g, 6 mol %) and copper(I) iodide (0.009 g, 11 mol %) were added. The mixture was heated to 50 °C and stirred for 24 h. Afterward, the mixture was vacuum-filtered with celite, diluted with ethyl acetate (15 mL), extracted with water (3 × 30 mL) and brine (2 × 30 mL), and dried over sodium sulfate. The concentrated mixture was purified by combiflash with ethyl acetate (10%)/hexane (90%) as the eluting solvent to yield the product as an oil (0.0623 g, 67%).

^{1}H NMR (400 MHz, $CDCl_3$): δ 7.66 (ddd, J = 7.8, 1.5, 0.5 Hz, 1H), 7.47 (ddd, J = 7.7, 1.4, 0.4 Hz, 1H), 7.39 (td, J = 7.5, 1.5 Hz, 1H), 7.32 (td, J = 7.6, 1.4 Hz, 1H), 2.83 (7, J = 6.9 Hz, 1H), 2.73 (s,

https://dx.doi.org/10.1021/acs.joc.0c02318
J. Org. Chem. 2021, 86, 693−708

3H), 1.28 (d, J = 6.9 Hz, 6H). ^{13}C NMR (101 MHz, $CDCl_3$): δ 201.3, 141.2, 134.0, 131.2, 128.4, 127.7, 122.5, 102.1, 79.2, 30.3, 22.7, 21.6. HRMS (CI): m/z calculated for $C_{13}H_{15}O$ [M + H], 187.1117; found, 187.1118.

Synthesis of *o*-Arylalkynylbenzaldehyde and Acetophenone *O*-Methyl Oximes. A 40 mL vial fitted with screw-top septa and equipped with a stirring magnet was charged with the aldehyde (1 equiv), methoxylamine hydrochloride (CH_3ONH_2·HCl, 98%, 2 equiv), and solid sodium acetate (NaOAc, 4.5 equiv) or sodium hydroxide (NaOH, 4.5 equiv) before dissolution in 20 mL of 50% ethanol in water. The mixture was stirred and heated at 85 °C. Reaction progress was monitored by TLC, and the heating was ceased once conversion to the product occurred. The mixture was cooled to room temperature and extracted with dichloromethane (DCM) (3 × 20 mL). The solvent was removed by concentrating *in vacuo*, and the crude product was dried under vacuum. In some cases, products were purified by dry column chromatography (ether/hexane). Products were characterized by gas chromatography mass spectrometry (GC−MS) and nuclear magnetic resonance spectroscopy (^{1}H NMR and ^{13}C NMR).

*(E)-2-(Phenylethynyl)benzaldehyde O-Methyl Oxime (**1**).*[34] 2-(Phenylethynyl)benzaldehyde (0.4113 g, 2.0 mmol, and 1 mol equiv), methoxylamine hydrochloride (249 μL, 1.6 mol equiv), and pyridine (264 μL, 2 mol equiv) were stirred in ethanol (8.2 mL) for 2 h. The solvent was removed *in vacuo*, and the residue was diluted with ethyl acetate (15 mL), extracted with deionized water (2 × 15 mL) and brine (2 × 15 mL), and dried over sodium sulfate. The concentrated mixture was purified by combiflash using ethyl acetate (10%)/hexane (90%) as the eluting solvent to yield the desired product as a yellow oil (0.2578 g, 67%). ^{1}H NMR (400 MHz, $CDCl_3$): δ 8.66 (s, 1H), 7.95−7.90 (m, 1H), 7.57−7.52 (m, 3H), 7.38−7.32 (m, 5H), 4.01 (s, 3H). ^{13}C NMR (101 MHz, $CDCl_3$): δ 147.43, 133.35, 132.64, 131.74, 129.58, 128.78, 128.65, 128.55, 125.37, 123.14, 122.97, 94.96, 86.42, 62.30.

*(E)-1-(2-(Phenylethynyl)phenyl)ethanone O-Methyl Oxime (**3**).*[50] 1-(2-(2-Phenylethynyl)phenyl)ethanone (0.5965 g, 2.7 mmol, and 1 mol equiv), methoxylamine hydrochloride (410 μL, 2 mol equiv), and pyridine (435 μL, 2 mol equiv) were stirred in ethanol (10 mL) for 2 h. The solvent was removed *in vacuo*, and the residue was diluted with ethyl acetate (15 mL), extracted with deionized water (2 × 15 mL) and brine (2 × 15 mL), and dried over sodium sulfate. The concentrated mixture was purified by combiflash using ethyl acetate (20%)/hexane (80%) as the eluting solvent to yield the desired product as a yellow oil (0.4950 g, 73%). ^{1}H NMR (400 MHz, $CDCl_3$): δ 7.59−7.55 (m, 1H), 7.52−7.49 (m, 2H), 7.42−7.40 (m, 1H), 7.37−7.33 (m, 5H), 4.01 (s, 3H), 2.36 (s, 3H).^{13}C NMR (101 MHz, $CDCl_3$): δ 156.95, 140.16, 133.11, 131.57, 128.59, 128.57, 128.53, 123.38, 121.84, 118.08, 116.95, 93.74, 88.30, 62.07, 16.18.

Synthesis of *o*-Arylalkynylacetophenone Oximes. To a stirring solution of *o*-arylalkynyl acetophenone (2.3 mmol, 1 equiv) in ethanol (20 mL), hydroxylamine hydrochloride (1.5 equiv) and pyridine (2 equiv) were added. The reaction was stirred at room temperature for 2 h and then concentrated *in vacuo*. Afterward, the residue was diluted with ethyl acetate, extracted with water, and dried over sodium sulfate. The dried organic layer was concentrated *in vacuo* and purified with combiflash by using an ethyl acetate/hexane mixture as the eluting solvent.

*(E)-2-(Phenylethynyl)benzaldehyde Oxime (**2**).*[30] 2-(Phenylethynyl)benzaldehyde (0.4376 g, 2.1 mmol, and 1 mol equiv), hydroxylamine hydrochloride (0.2427 g, 1.6 mol equiv) and pyridine (280 μL, 1.3 mol equiv) were stirred in ethanol (8.7 mL) for 2 h. After workup, the mixture was purified by combiflash using an ethyl acetate (35%)/hexane (65%) mixture as the eluting solvent to yield the desired product as a white solid (0.3009 g, 78%). ^{1}H NMR (400 MHz, $CDCl_3$): δ 8.77 (s, 1H), 8.66 (s, 1H), 7.90−7.87 (m, 1H), 7.59−7.55 (m, 3H), 7.40−7.33 (m, 5H). ^{13}C NMR (101 MHz, $CDCl_3$): δ 149.21, 133.04, 132.73, 131.74, 129.84, 128.83, 128.72, 128.55, 125.32, 123.33, 122.85, 95.17, 86.30.

*(E)-1-(2-(Phenylethynyl)phenyl)ethanone Oxime (**4a**).*[33] 1-(2-(2-Phenylethynyl)phenyl)ethanone (0.9521 g, 4.33 mmol), hydroxylamine hydrochloride (0.6025 g, 2 mol equiv) and pyridine (280 μL, 0.8 mol equiv) were stirred in methanol (22 mL) for 2 h. After workup, the mixture was purified by combiflash using an ethyl acetate (35%)/hexane (65%) mixture as the eluting solvent to yield the desired product as an off-white solid (0.9041 g, 88%). ^{1}H NMR (400 MHz, $CDCl_3$): δ 9.40 (s, 1H, br), 7.61−7.59 (m, 1H), 7.53−7.50 (m, 2H), 7.43−7.31 (m, 6H), 2.40 (s, 3H). ^{13}C NMR (101 MHz, $CDCl_3$): δ 157.6, 140.0, 133.2, 131.7, 128.70, 128.57, 128.53, 128.47, 128.41, 123.3, 121.8, 93.8, 88.2, 15.6.

*(E)-1-(2-(Hex-1-yn-1-yl)phenyl)ethanone Oxime (**4b**).*[33] 1-(2-(Hex-1-yn-1-yl)phenyl)ethanone (0.300 g, 1.5 mmol), hydroxylamine hydrochloride (0.1570 g, 1.5 mol equiv), and sodium acetate (0.1344 g, 1.1 mol equiv) were stirred in methanol (20 mL) for 24 h. After workup, the mixture was purified by column chromatography to yield the desired product as an off-white solid (0.254 g, 85%). ^{1}H NMR (400 MHz, $CDCl_3$): δ 8.15 (s, 1H), 7.46−7.41 (m, 1H), 7.33−7.26 (m, 3H), 2.41 (t, J = 7.0 Hz, 2H), 2.32 (s, 3H), 1.62−1.55 (m, 2H), 1.51−1.42 (m, 2H), 0.94 (t, J = 7.3 Hz, 3H). ^{13}C NMR (101 MHz, $CDCl_3$): δ 158.5, 140.0, 133.2, 128.6, 128.3, 127.7, 122.7, 95.3, 79.2, 30.8, 22.2, 19.4, 15.5, 13.8.

*(E)-1-(2-(3-Methylbut-1-yn-1-yl)phenyl)ethanone Oxime (**4c**).* 1-(2-(3-Methylbut-1-ynyl)phenyl)ethanone (0.5635 g, 2.97 mmol), hydroxylamine hydrochloride (0.4132 g, 2 mol equiv), and pyridine (478 μL, 2 mol equiv) were stirred in methanol (15 mL) for 2 h. After workup, the mixture was purified by combiflash using an ethyl acetate (35%)/hexane (65%) mixture as the eluting solvent to yield the desired product as an off-white solid (0.4888 g, 80%). ^{1}H NMR (400 MHz, $CDCl_3$): δ 8.46 (s, 1H), 7.45−7.41 (m, 1H), 7.33−7.30 (m, 1H), 7.29−7.26 (m, 2H), 2.78 (7, J = 6.9 Hz, 1H), 2.33 (s, 3H), 1.25 (d, J = 6.9 Hz, 6H). ^{13}C NMR (101 MHz, $CDCl_3$): δ 158.1, 140.0, 133.1, 128.5, 128.3, 127.7, 122.6, 100.5, 78.5, 22.9, 21.4, 15.5. HRMS (CI): m/z calculated for $C_{13}H_{16}NO$ [M + H], 202.1226; found, 202.1226.

Photolysis of *o*-Arylalkynyloximes with DCA in Acetonitrile-d_3. A nuclear magnetic resonance (NMR) tube was charged with 9,10-dicyanoanthracene (DCA) (5 μM), the oxime or oxime ether (15 μM), and 1 mL of acetonitrile-d_3 (CD_3CN). The samples were photolyzed at 420 nm using a photoreactor equipped with 10 mercury vapor lamps for a total of 4 h, unless otherwise noted. NMR analysis was performed every hour. For quantification, an internal standard of either 4-nitrobenzyl-bromide or 4-nitrobenzaldehyde was added following photolysis to determine product yield by ^{1}H NMR. Product isolation conditions: Once removed from the photoreactor, the contents of multiple (5−20) NMR tubes were combined, and residual DCA was removed by vacuum filtration. The solvent was evaporated *in vacuo*, and the residue was purified by flash chromatography using dichloromethane and acetonitrile to yield the pure product that was characterized by NMR.

*(E)-1-Benzylidene-3-methyl-1H-isoindole 2-oxide (**5a**).* ^{1}H NMR (400 MHz, $CDCl_3$): δ 8.14 (s, 1H), 7.64−7.60 (m, 3H), 7.51−7.45 (m, 3H), 7.35−7.28 (m, 2H), 7.17 (td, J = 7.4, 1.4 Hz, 1H), 2.48 (s, 3H). ^{13}C NMR (101 MHz, $CDCl_3$): δ 142.79, 141.38, 134.87, 133.02, 129.84, 129.70, 128.92, 128.85, 128.16, 126.71, 121.83, 119.22, 9.76. HRMS (CI): m/z calculated for $C_{16}H_{14}NO$ [M + H], 236.1070; found, 236.1069.

*(E)-3-Methyl-1-(2-methylpropylidene)-1H-isoindole 2-Oxide (**5c**).* ^{1}H NMR (400 MHz, $CDCl_3$): δ 7.63−7.61 (m, 1H), 7.35−7.28 (m, 3H), 7.06 (d, J = 10.6 Hz, 1H), 3.41−3.28 (m, 1H), 2.41 (s, 3H), 1.25 (d, J = 6.7 Hz, 6H). ^{13}C NMR (101 MHz, $CDCl_3$): δ 142.23, 139.84, 138.32, 134.35, 128.84, 128.15, 127.26, 122.11, 119.19, 27.10, 22.40, 9.53. HRMS (CI): m/z calculated for $C_{13}H_{15}NO$ [M + H], 202.1226; found, 202.1227.

Ag(I)-Catalyzed Oxidative Cyclization Reactions of *o*-Arylalkynyloximes. A round-bottom flask was charged with the oxime (0.27 mmol), dichloromethane (2 mL), and silver triflate (2.7 mmol). The sample was stirred for 40 min, and the reaction was followed by TLC. The solvent was removed *in vacuo*, and the residue was purified by column chromatography using a DCM−methanol gradient. Removal of the solvent yielded the solid product, which was analyzed by ^{1}H NMR.

https://dx.doi.org/10.1021/acs.joc.0c02318
J. Org. Chem. 2021, 86, 693−708

*1-Methyl-3-phenylisoquinoline 2-Oxide (**6a**).*[33] ^{1}H NMR (400 MHz, $CDCl_3$): δ 7.96 (dd, J = 8.6, 0.8 Hz, 1H), 7.79−7.77 (m, 3H), 7.68 (s, 1H), 7.63 (ddd, J = 8.4, 7.0, 1.4 Hz, 1H), 7.56 (ddd, J = 8.0, 7.0, 1.1 Hz, 1H), 7.52−7.45 (m, 3H), 2.95 (s, 3H).

*3-Butyl-1-methylisoquinoline 2-Oxide (**6b**).*[33] ^{1}H NMR (400 MHz, $CDCl_3$): δ 7.91 (dd, J = 8.7, 0.8 Hz, 1H), 7.71 (dd, J = 7.2, 2.0 Hz, 1H), 7.58−7.50 (m, 2H), 7.48 (s, 1H), 3.06 (t, J = 7.7 Hz, 2H), 2.91 (s, 3H), 1.83−1.76 (m, 2H), 1.50 (dq, J = 14.9, 7.4 Hz, 2H), 1.00 (t, J = 7.4 Hz, 3H); ^{13}C NMR (101 MHz, $CDCl_3$): δ 149.2, 145.6, 128.7, 128.0, 127.9, 127.6, 126.9, 123.9, 119.9, 30.9, 29.2, 22.8, 14.1, 13.6.

COMPUTATIONAL METHODS

Calculation of the ^{1}H and ^{13}C NMR chemical shifts began by obtaining optimized geometries in the gas phase using DFT at the B3LYP/6-31+G(d,p) level of theory with a pruned (99,590) grid. NMR isotropic shielding tensors were calculated at these optimized geometries using the gauge including atomic orbital (GIAO) method with solvent effects included through an integral equation formalism polarizable continuum model (IEF-PCM) parameterized for chloroform with the cavity constructed using UFF atomic radii.[51−53] The NMR isotropic shielding tensors for ^{1}H were calculated at the mPW1PW91/6-311+G(2d,p) level of theory, whereas these calculations were performed at the B3LYP/6-311+G(2d,p) level of theory for ^{13}C. A pruned (99,590) grid was used for all of these calculations. For **5b**, where the experimental ^{1}H NMR spectrum was measured in acetonitrile, the NMR isotropic shielding tensors for ^{1}H were calculated at the WP04/aug-cc-pvdz level of theory with the IEF-PCM parameterized for acetonitrile. Finally, the calculated NMR isotropic shielding tensors were converted into NMR chemical shifts using the calibration curves developed by Pierens.[42] These calculations were performed using Gaussian 09.[54]

Calculation of the neutral, radical, and radical cation stationary points followed the same computational procedure as our previous study of the 2′-arylbenzaldehyde oxime ethers.[43] Specifically, we began with gas phase geometry optimizations performed at the ωB97X-D/cc-pVDZ level of theory with an (99,590) integration grid.[55,56] An unrestricted formalism was used for the radicals and radical cations. Vibrational frequency analysis at the stationary points showed that all minima had no imaginary frequencies, whereas all transition states only had a single imaginary frequency with a vibrational motion consistent with the expected reaction coordinate. Single-point calculations were performed at the optimized geometries using the ωB97M-V/def2-QZVPP level of theory with a (99,590) grid for the local exchange-correlation and an SG-1 grid for the nonlocal correlation.[57,58] These single-point calculations included solvent effects through an IEF-PCM parameterized for acetonitrile with the cavity constructed using Bondi radii and switching Gaussian surface charges.[51,59,60] The single-point calculations were performed in the restricted open-shell formalism for the radicals and radical cations. The single-point electronic energies were combined with the harmonic enthalpy and entropy to calculate the free energy at T = 298.15 K. All of these calculations were performed using the Q-Chem 5.1 package.[61]

The ionization potentials were calculated as the difference in the electronic energy of the radical cation and the neutral states at the neutral optimized geometries. The ionization potentials were thermally averaged over all relevant neutral molecular conformations using the Boltzmann distributions. This thermal averaging included conformations with the oxime group oriented toward and away from the alkynyl group.

The pK_a of the oxime radical cations, ROH$^{\cdot+}$, were estimated using the equation

$$pK_a(ROH^{\cdot+}) = pK_a(CH_3COOH) + \frac{\Delta G}{2.303RT}$$

where[62,63]

$$\Delta G = \Delta G_{gas}(ROH^{\cdot+}) - \Delta G_{gas}(CH_3COOH) + \Delta G_{solv}(RO\cdot) + \Delta G_{solv}(CH_3COOH) - \Delta G_{solv}(ROH^{\cdot+}) - \Delta G_{solv}(CH_3COO^-)$$

Here, $\Delta G_{gas}(ROH^{\cdot+})$ is the gas phase free energy of the reaction $ROH^{\cdot+} \rightarrow RO^{\cdot} + H^+$ calculated at the m06-2X/6-311++G(d,p) level of theory with a (99,590) grid. The gas phase free energy of the proton is −6.28 kcal/mol. The solvation free energy, $\Delta G_{solv}(ROH^{\cdot+})$, was calculated using the SM12 solvation model with ChElPG charges and parameters for acetonitrile;[64] the same m06-2X/6-311++G(d,p) level of theory with a (99,590) grid was used for these calculations. In the above analysis, acetic acid is used as a reference acid, and we use the literature value for pK_a(CH_3COOH) in acetaldehyde, 23.51.[65]

ASSOCIATED CONTENT

Supporting Information

The Supporting Information is available free of charge at https://pubs.acs.org/doi/10.1021/acs.joc.0c02318.

Comparison of the ^{1}H NMR spectra of **5a−5c** and **6a−6c**, detailed comparison of experimental and computational NMR chemical shifts of **6a−6c** and **5b−5c**, spin densities of the **4a−4c** radical cations, calculated pK_a values for **3** and **4a−4c** radical cations as well as their 5-exo radical cation intermediates, radical and radical cation cyclization reaction coordinate diagrams for **3** and **4b−4c**, NBO analysis of the radical and the radical cation forms of **4a−4c**, neutral reaction coordinate diagrams for the ring opening reactions of the 5-exo trans and 6-endo intermediates of **4a−4c**, and radical cation and neutral reaction coordinate diagrams for **2** (PDF)

Experimental NMR spectra for all new compounds as well as HRMS data, raw thermodynamic information along with the geometries of all molecular conformations considered in this study (PDF)

AUTHOR INFORMATION

Corresponding Authors

Andrew S. Petit − *Department of Chemistry and Biochemistry, California State University, Fullerton, California 92834-6866, United States;* orcid.org/0000-0002-9428-3499; Email: apetit@fullerton.edu

H. J. Peter de Lijser − *Department of Chemistry and Biochemistry, California State University, Fullerton, California 92834-6866, United States*; Email: pdelijser@fullerton.edu

Authors

Wan Shin Kim − *Department of Chemistry and Biochemistry, California State University, Fullerton, California 92834-6866, United States*

Victor M. Espinoza Castro − *Department of Chemistry and Biochemistry, California State University, Fullerton, California 92834-6866, United States*

Amanda Abiad − *Department of Chemistry and Biochemistry, California State University, Fullerton, California 92834-6866, United States*

Michael Ko − *Department of Chemistry and Biochemistry, California State University, Fullerton, California 92834-6866, United States*

Ashley Council − *Department of Chemistry and Biochemistry, California State University, Fullerton, California 92834-6866, United States*

https://dx.doi.org/10.1021/acs.joc.0c02318
J. Org. Chem. 2021, 86, 693−708

Anh Nguyen − *Department of Chemistry and Biochemistry, California State University, Fullerton, California 92834-6866, United States*
Laura Marsalla − *Department of Chemistry and Biochemistry, California State University, Fullerton, California 92834-6866, United States*
Vicky Lee − *Department of Chemistry and Biochemistry, California State University, Fullerton, California 92834-6866, United States*
Thao Tran − *Department of Chemistry and Biochemistry, California State University, Fullerton, California 92834-6866, United States*

Complete contact information is available at: https://pubs.acs.org/10.1021/acs.joc.0c02318

Notes

The authors declare no competing financial interest.

■ ACKNOWLEDGMENTS

Acknowledgement is made to the donors of the Petroleum Research Fund, administered by the American Chemical Society (53793-UR4 and 59497-UNI4). This research was supported by the National Science Foundation under grant no. CHE-0844110 and by start-up funds granted by the College of Natural Sciences and Mathematics at the California State University, Fullerton. Instrumentation support was provided by the National Science Foundation MRI (CHE1726903) for acquisition of a UPLC-MS. This work used the Extreme Science and Engineering Discovery Environment (XSEDE), which is supported by the National Science Foundation grant number ACI-1548562. This work specifically used the Comet cluster at the San Diego Supercomputer Center through allocation TG-CHE180057. Additional computational resources were provided through the Center for Computational and Applied Mathematics at the California State University, Fullerton. We thank Ms. Jovy Trejo for her contributions to the synthesis of some of the compounds and Dr. Paula K. Hudson for her assistance with the collection and analysis of the HRMS data.

■ REFERENCES

(1) Tanase, S.; Hierso, J.-C.; Bouwman, E.; Reedijk, J.; ter Borg, J.; Bieleman, J. H.; Schut, A. New Insights on the Anti-Skinning Effect of Methyl Ethyl Ketoxime in Alkyd Paints. *New J. Chem.* **2003**, *27*, 854−859.
(2) Bieleman, J.; Glaser, J. K.; Spang, R.; Bolle, T.; Braig, A.; Köhler, M.; Valet, A. Additives for Special Functions. In *Additives for Coatings*; Wiley: 2000; pp. 257−352, DOI: 10.1002/9783527613304.ch8.
(3) Vangorkum, R.; Bouwman, E. The Oxidative Drying of Alkyd Paint Catalysed by Metal Complexes. *Coord. Chem. Rev.* **2005**, *249*, 1709−1728.
(4) Yamada, H.; Yoneyama, F.; Satoh, K.; Taira, N. Comparison of the Effects of the Novel Vasodilator FK409 with Those of Nitroglycerin in Isolated Coronary Artery of the Dog. *Br. J. Pharmacol.* **1991**, *103*, 1713−1718.
(5) Isono, T.; Koibuchi, Y.; Sato, N.; Furuichi, A.; Nishii, M.; Yamamoto, T.; Mori, J.; Kohsaka, M.; Ohtsuka, M. Vasorelaxant Mechanism of the New Vasodilator, FK409. *Eur. J. Pharmacol. Mol. Pharmacol.* **1993**, *246*, 205−212.
(6) Kita, Y.; Hirasawa, Y.; Maeda, K.; Nishio, M.; Yoshida, K. Spontaneous Nitric Oxide Release Accounts for the Potent Pharmacological Actions of FK409. *Eur. J. Pharmacol.* **1994**, *257*, 123−130.
(7) Venhuis, B. J.; Dijkstra, D.; Wustrow, D.; Meltzer, L. T.; Wise, L. D.; Johnson, S. J.; Wikström, H. V. Orally Active Oxime Derivatives of the Dopaminergic Prodrug 6-(N,N-Di-n-Propylamino)-3,4,5,6,7,8-Hexahydro-2H-Naphthalen-1-One. Synthesis and Pharmacological Activity. *J. Med. Chem.* **2003**, *46*, 4136−4140.
(8) Dimmock, J. R.; Sidhu, K. K.; Chen, M.; Li, J.; Quail, J. W.; Allen, T. M.; Kao, G. Y. Synthesis and Cytotoxic Evaluation of Some Cyclic Arylidene Ketones and Related Oximes, Oxime Esters, and Analogs. *J. Pharm. Sci.* **1994**, *83*, 852−858.
(9) Buckley, N. A.; Eddleston, M.; Li, Y.; Bevan, M.; Robertson, J. Oximes for Acute Organophosphate Pesticide Poisoning. *Cochrane Database Syst. Rev.* **2011**, DOI: 10.1002/14651858.CD005085.pub2.
(10) Eddleston, M.; Eyer, P.; Worek, F.; Juszczak, E.; Alder, N.; Mohamed, F.; Senarathna, L.; Hittarage, A.; Azher, S.; Jeganathan, K.; Jayamanne, S.; von Meyer, L.; Dawson, A. H.; Sheriff, M. H. R.; Buckley, N. A. Pralidoxime in Acute Organophosphorus Insecticide Poisoning—A Randomised Controlled Trial. *PLoS Med.* **2009**, *6*, No. e1000104.
(11) Jokanovic, M.; Prostran, M. Pyridinium Oximes as Cholinesterase Reactivators. Structure-Activity Relationship and Efficacy in the Treatment of Poisoning with Organophosphorus Compounds. *Curr. Med. Chem.* **2009**, *16*, 2177−2188.
(12) Clement, J. G. HI-6: Reactivation of Central and Peripheral Acetylcholinesterase Following Inhibition by Soman, Sarin and Tabun in Vivo in the Rat. *Biochem. Pharmacol.* **1982**, *31*, 1283−1287.
(13) Abele, E.; Abele, R. Recent Advances in the Synthesis of Heterocycles from Oximes (2014-2017). *Curr. Org. Chem.* **2018**, *22*, 1486−1504.
(14) Abele, E.; Abele, R. Recent Advances in the Synthesis of Heterocycles from Oximes. *Curr. Org. Synth.* **2014**, *11*, 403−428.
(15) Rossi, R.; Bardagi, J.; Buden, M. Constructing Heterocycles by Visible Light Photocatalysis. *Curr. Org. Synth.* **2017**, *14*, 398−429.
(16) Walton, J. C. Functionalised Oximes: Emergent Precursors for Carbon-,Nitrogen- and Oxygen-Centred Radicals. *Molecules* **2016**, *21*, 63−75.
(17) Vitale, P.; Scilimati, A. Recent Developments in the Chemistry of 3-Arylisoxazoles and 3-Aryl-2-Isoxazolines. In *Advances in Heterocyclic Chemistry*; Academic Press: 2017; Vol. *122*, pp. 1−41, DOI: 10.1016/bs.aihch.2016.10.001.
(18) He, L.; Nie, H.; Qiu, G.; Gao, Y.; Wu, J. 2-Alkynylbenzaldoxime: A Versatile Building Block for the Generation of N-Heterocycles. *Org. Biomol. Chem.* **2014**, *12*, 9045−9053.
(19) Ueda, M.; Sato, A.; Ikeda, Y.; Miyoshi, T.; Naito, T.; Miyata, O. Direct Synthesis of Trisubstituted Isoxazoles through Gold-Catalyzed Domino Reaction of Alkynyl Oxime Ethers. *Org. Lett.* **2010**, *12*, 2594−2597.
(20) Ding, Q.; Wang, Z.; Wu, J. Tandem Cyclization-[3+3] Cycloaddition Reactions of 2-Alkynylbenzaldoxime: Synthesis of Fused 1,2-Dihydroisoquinolines. *Tetrahedron Lett.* **2009**, *50*, 198−200.
(21) Li, J.; Hu, Y.; Zhang, D.; Liu, Q.; Dong, Y.; Liu, H. Transition Metal-Catalyzed Reactions Involving Oximes. *Adv. Synth. Catal.* **2017**, *359*, 710−771.
(22) Hofstra, J. L.; Grassbaugh, B. R.; Tran, Q. M.; Armada, N. R.; de Lijser, H. J. P. Catalytic Oxidative Cyclization of 2′-Arylbenzaldehyde Oxime Ethers under Photoinduced Electron Transfer Conditions. *J. Org. Chem.* **2015**, *80*, 256−265.
(23) de Lijser, H. J. P.; Tsai, C.-K. Photosensitized Reactions of Oxime Ethers: A Steady-State and Laser Flash Photolysis Study. *J. Org. Chem.* **2004**, *69*, 3057−3067.
(24) de Lijser, H. J. P.; Hsu, S.; Marquez, B. V.; Park, A.; Sanguantrakun, N.; Sawyer, J. R. Effect of Structure in Benzaldehyde Oximes on the Formation of Aldehydes and Nitriles under Photoinduced Electron-Transfer Conditions. *J. Org. Chem.* **2006**, *71*, 7785−7792.
(25) de Lijser, H. J. P.; Burke, C. R.; Rosenberg, J.; Hunter, J. Highly Efficient Formation of Nitriles and Alkoxy Radicals from N -Alkoxybenziminoyl Chlorides in Solution. *J. Org. Chem.* **2009**, *74*, 1679−1684.

(26) Park, A.; Kosareff, N. M.; Kim, J. S.; de Lijser, H. J. P. Quinone-Sensitized Steady-State Photolysis of Acetophenone Oximes Under Aerobic Conditions: Kinetics and Product Studies†. *Photochem. Photobiol.* **2006**, *82*, 110.
(27) de Lijser, H. P.; Kim, J. S.; McGrorty, S. M.; Ulloa, E. M. Substituent Effects in Oxime Radical Cations. 1. Photosensitized Reactions of Acetophenone Oximes. *Can. J. Chem.* **2003**, *81*, 575−585.
(28) Sakamoto, T.; Numata, A.; Kondo, Y. The Cyclization Reaction of Ortho-Ethynylbenzaldehyde Derivatives into Isoquinoline Derivatives. *Chem. Pharm. Bull.* **2000**, *48*, 669−672.
(29) Yamanaka, H.; Sakamoto, T.; Kondo, Y.; Miura, N.; Hayashi, K. Condensed Heteroaromatic Ring Systems. XI. A Facile Synthesis of Isoquinoline N-Oxides. *Heterocycles* **1986**, *24*, 2311−2314.
(30) Ding, Q.; Wu, J. Access to Functionalized Isoquinoline N -Oxides via Sequential Electrophilic Cyclization/Cross-Coupling Reactions. *Adv. Synth. Catal.* **2008**, *350*, 1850−1854.
(31) Huo, Z.; Tomeba, H.; Yamamoto, Y. Iodine-Mediated Electrophilic Cyclization of 2-Alkynylbenzaldoximes Leading to the Formation of Iodoisoquinoline N-Oxides. *Tetrahedron Lett.* **2008**, *49*, 5531−5533.
(32) Yeom, H.-S.; Kim, S.; Shin, S. Silver(I)-Catalyzed Direct Route to Isoquinoline- N -Oxides. *Synlett* **2008**, *2008*, 924−928.
(33) Yeom, H.-S.; Lee, Y.; Lee, J.-E.; Shin, S. Geometry-Dependent Divergence in the Gold-Catalyzed Redox Cascade Cyclization of o-Alkynylaryl Ketoximes and Nitrones Leading to Isoindoles. *Org. Biomol. Chem.* **2009**, *7*, 4744−4752.
(34) Gao, H.; Zhang, J. A Dramatic Substituent Effect in Silver(I)-Catalyzed Regioselective Cyclization of Ortho-Alkynylaryl Aldehyde Oxime Derivatives. *Adv. Synth. Catal.* **2009**, *351*, 85−88.
(35) Qiu, G.; Ding, Q.; Ren, H.; Peng, Y.; Wu, J. Multicatalytic One-Pot Reaction of 1-(2-Alkynylphenyl)Ketoximes for Generation of Indole Derivatives. *Org. Lett.* **2010**, *12*, 3975−3977.
(36) Deb, I.; Yoshikai, N. Phenanthridine Synthesis through Iron-Catalyzed Intramolecular N -Arylation of O -Acetyl Oxime. *Org. Lett.* **2013**, *15*, 4254−4257.
(37) Miyaura, N.; Yamada, K.; Suzuki, A. A New Stereospecific Cross-Coupling by the Palladium-Catalyzed Reaction of 1-Alkenylboranes with 1-Alkenyl or 1-Alkynyl Halides. *Tetrahedron Lett.* **1979**, *20*, 3437−3440.
(38) Ye, F.; Shi, Y.; Zhou, L.; Xiao, Q.; Zhang, Y.; Wang, J. Expeditious Synthesis of Phenanthrenes via CuBr 2 -Catalyzed Coupling of Terminal Alkynes and N- Tosylhydrazones Derived from O -Formyl Biphenyls. *Org. Lett.* **2011**, *13*, 5020−5023.
(39) Rhodes, C. J.; Agirbas, H. Electron Paramagnetic Resonance Study of Imine Radical Cations in Low-Temperature Solid Matrices. *J. Chem. Soc., Faraday Trans.* **1990**, *86*, 3303.
(40) Bordwell, F. G.; Ji, G. Z. Equilibrium Acidities and Homolytic Bond Dissociation Energies of the H-O Bonds in Oximes and Amidoximes. *J. Org. Chem.* **1992**, *57*, 3019−3025.
(41) Product **5a** showed some signs of minor decomposition over time, but this process occurred both under the photochemical conditions of the reaction as well as in the absence of light (thermal). Even though NMR analysis seemed to suggest that compound **5a** was converted into a different product, we have not yet been able to identify this degradation product.
(42) Pierens, G. K. ^{1}H and ^{13}C NMR Scaling Factors for the Calculation of Chemical Shifts in Commonly Used Solvents Using Density Functional Theory. *J. Comput. Chem.* **2014**, *35*, 1388−1394.
(43) Ulloa, L. K.; Kong, S.; Vigil, A. M.; Petit, A. S. Computational Investigation of Substituent Effects on the Formation and Intramolecular Cyclization of 2′-Arylbenzaldehyde and 2′-Arylacetophenone Oxime Ether Radical Cations. *J. Org. Chem.* **2019**, *84*, 14659−14669.
(44) Rehm, D.; Weller, A. Kinetics of Fluorescence Quenching by Electron and H-Atom Transfer. *Isr. J. Chem.* **1970**, *8*, 259−271.
(45) Gould, I. R.; Ege, D.; Moser, J. E.; Farid, S. Efficiencies of Photoinduced Electron-Transfer Reactions: Role of the Marcus Inverted Region in Return Electron Transfer within Geminate Radical-Ion Pairs. *J. Am. Chem. Soc.* **1990**, *112*, 4290−4301.
(46) Glendening, E. D.; Landis, C. R.; Weinhold, F. Natural Bond Orbital Methods. *Wiley Interdiscip. Rev.: Comput. Mol. Sci.* **2012**, *2*, 1−42.
(47) Nicholson, R. S.; Shain, I. Theory of Stationary Electrode Polarography. Single Scan and Cyclic Methods Applied to Reversible, Irreversible, and Kinetic Systems. *Anal. Chem.* **1964**, *36*, 706−723.
(48) Nicholson, R. S.; Shain, I. Theory of Stationary Electrode Polarography for a Chemical Reaction Coupled between Two Charge Transfers. *Anal. Chem.* **1965**, *37*, 178−190.
(49) Yanada, R.; Hashimoto, K.; Tokizane, R.; Miwa, Y.; Minami, H.; Yanada, K.; Ishikura, M.; Takemoto, Y. Indium(III)-Catalyzed Tandem Reaction with Alkynylbenzaldehydes and Alkynylanilines to Heteroaromatic Compounds. *J. Org. Chem.* **2008**, *73*, 5135−5138.
(50) Xie, F.; Zhang, Z.; Yu, X.; Tang, G.; Li, X. Diaryliodoniums by Rhodium(III)-Catalyzed C-H Activation: Mild Synthesis and Diversified Functionalizations. *Angew. Chem., Int. Ed.* **2015**, *54*, 7405−7409.
(51) Tomasi, J.; Mennucci, B.; Cammi, R. Quantum Mechanical Continuum Solvation Models. *Chem. Rev.* **2005**, *105*, 2999−3094.
(52) Ditchfield, R. Self-Consistent Perturbation Theory of Diamagnetism. *Mol. Phys.* **1974**, *27*, 789−807.
(53) Wolinski, K.; Hinton, J. F.; Pulay, P. Efficient Implementation of the Gauge-Independent Atomic Orbital Method for NMR Chemical Shift Calculations. *J. Am. Chem. Soc.* **1990**, *112*, 8251−8260.
(54) Frisch, M. J. E. A.; Trucks, G. W.; Schlegel, H. B.; Scuseria, G. E.; Robb, M. A.; Cheeseman, J. R.; Scalmani, G.; Barone, V.; Mennucci, B.; Petersson, G.; Nakatsuji, H. *Gaussian 09*, Revision B.01. Gaussian, Inc.: Wallingford, CT 2016.
(55) Chai, J.-D.; Head-Gordon, M. Long-Range Corrected Hybrid Density Functionals with Damped Atom−Atom Dispersion Corrections. *Phys. Chem. Chem. Phys.* **2008**, *10*, 6615−6620.
(56) Chai, J.-D.; Head-Gordon, M. Systematic Optimization of Long-Range Corrected Hybrid Density Functionals. *J. Chem. Phys.* **2008**, *128*, No. 084106.
(57) Mardirossian, N.; Head-Gordon, M. Mapping the Genome of Meta-Generalized Gradient Approximation Density Functionals: The Search for B97M-V. *J. Chem. Phys.* **2015**, *142*, No. 074111.
(58) Mardirossian, N.; Head-Gordon, M. ωB97M-V: A Combinatorially Optimized, Range-Separated Hybrid, Meta-GGA Density Functional with VV10 Nonlocal Correlation. *J. Chem. Phys.* **2016**, *144*, 214110.
(59) Lange, A. W.; Herbert, J. M. Polarizable Continuum Reaction-Field Solvation Models Affording Smooth Potential Energy Surfaces. *J. Phys. Chem. Lett.* **2010**, *1*, 556−561.
(60) Lange, A. W.; Herbert, J. M. A Smooth, Nonsingular, and Faithful Discretization Scheme for Polarizable Continuum Models: The Switching/Gaussian Approach. *J. Chem. Phys.* **2010**, *133*, 244111.
(61) Shao, Y.; Gan, Z.; Epifanovsky, E.; Gilbert, A. T. B.; Wormit, M.; Kussmann, J.; Lange, A. W.; Behn, A.; Deng, J.; Feng, X.; Ghosh, D.; Goldey, M.; Horn, P. R.; Jacobson, L. D.; Kaliman, I.; Khaliullin, R. Z.; Kuś, T.; Landau, A.; Liu, J.; Proynov, E. I.; Rhee, Y. M.; Richard, R. M.; Rohrdanz, M. A.; Steele, R. P.; Sundstrom, E. J.; Woodcock, H. L., III; Zimmerman, P. M.; Zuev, D.; Albrecht, B.; Alguire, E.; Austin, B.; Beran, G. J. O.; Bernard, Y. A.; Berquist, E.; Brandhorst, K.; Bravaya, K. B.; Brown, S. T.; Casanova, D.; Chang, C. M.; Chen, Y.; Chien, S. H.; Closser, K. D.; Crittenden, D. L.; Diedenhofen, M.; Distasio, R. A., Jr.; Do, H.; Dutoi, A. D.; Edgar, R. G.; Fatehi, S.; Fusti-Molnar, L.; Ghysels, A.; Golubeva-Zadorozhnaya, A.; Gomes, J.; Hanson-Heine, M. W. D.; Harbach, P. H. P.; Hauser, A. W.; Hohenstein, E. G.; Holden, Z. C.; Jagau, T.-C.; Ji, H.; Kaduk, B.; Khistyaev, K.; Kim, J.; Kim, J.; King, R. A.; Klunzinger, P.; Kosenkov, D.; Kowalczyk, T.; Krauter, C. M.; Lao, K. U.; Laurent, A. D.; Lawler, K. V.; Levchenko, S. V.; Lin, C. Y.; Liu, F.; Livshits, E.; Lochan, R. C.; Luenser, A.; Manohar, P.; Manzer, S. F.; Mao, S. P.; Mardirossian, N.; Marenich, A. V.; Maurer, S. A.; Mayhall, N. J.; Neuscamman, E.; Oana, C. M.; Olivares-Amaya, R.; O'neill, D. P.; Parkhill, J. A.; Perrine, T. M.; Peverati, R.; Prociuk, A.; Rehn, D. R.;

https://dx.doi.org/10.1021/acs.joc.0c02318
J. Org. Chem. 2021, 86, 693−708

Rosta, E.; Russ, N. J.; Sharada, S. M.; Sharma, S.; Small, D. W.; Sodt, A.; Stein, T.; Stück, D.; Su, Y.-C.; Thom, A. J. W.; Tsuchimochi, T.; Vanovschi, V.; Vogt, L.; Vydrov, O.; Wang, T.; Watson, M. A.; Wenzel, J.; White, A.; Williams, C. F.; Yang, J.; Yeganeh, S.; Yost, S. R.; You, Z.-Q.; Zhang, I. Y.; Zhang, X.; Zhao, Y.; Brooks, B. R.; Chan, G. K. L.; Chipman, D. M.; Cramer, C. J.; Goddard, W. A., III; Gordon, M. S.; Hehre, W. J.; Klamt, A.; Schaefer, H. F., III; Schmidt, M. W.; Sherrill, C. D.; Truhlar, D. G.; Warshel, A.; Xu, X.; Aspuru-Guzik, A.; Baer, R.; Bell, A. T.; Besley, N. A.; Chai, J.-D.; Dreuw, A.; Dunietz, B. D.; Furlani, T. R.; Gwaltney, S. R.; Hsu, C.-P.; Jung, Y.; Kong, J.; Lambrecht, D. S.; Liang, W.; Ochsenfeld, C.; Rassolov, V. A.; Slipchenko, L. V.; Subotnik, J. E.; Van Voorhis, T.; Herbert, J. M.; Krylov, A. I.; Gill, P. M. W.; Head-Gordon, M. Advances in Molecular Quantum Chemistry Contained in the Q-Chem 4 Program Package. *Mol. Phys.* **2015**, *113*, 184−215.

(62) Ding, F.; Smith, J. M.; Wang, H. First-Principles Calculation of pK_a Values for Organic Acids in Nonaqueous Solution. *J. Org. Chem.* **2009**, *74*, 2679−2691.

(63) Bryantsev, V. S.; Diallo, M. S.; Goddard, W. A. PK_a Calculations of Aliphatic Amines, Diamines, and Aminoamides via Density Functional Theory with a Poisson−Boltzmann Continuum Solvent Model. *J. Phys. Chem. A* **2007**, *111*, 4422−4430.

(64) Marenich, A. V.; Cramer, C. J.; Truhlar, D. G. Generalized Born Solvation Model SM12. *J. Chem. Theory Comput.* **2013**, *9*, 609−620.

(65) Kütt, A.; Leito, I.; Kaljurand, I.; Sooväli, L.; Vlasov, V. M.; Yagupolskii, L. M.; Koppel, I. A. A Comprehensive Self-Consistent Spectrophotometric Acidity Scale of Neutral Brønsted Acids in Acetonitrile. *J. Org. Chem.* **2006**, *71*, 2829−2838.

https://dx.doi.org/10.1021/acs.joc.0c02318
J. Org. Chem. 2021, 86, 693−708